

## RESEARCH ARTICLE

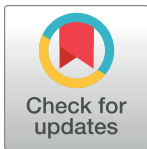
## Distinct functions of three chromatin remodelers in activator binding and preinitiation complex assembly

Yashpal Rawal<sup>1,2\*</sup>, Hongfang Qiu<sup>1</sup>, Alan G. Hinnebusch<sup>1,2\*</sup>

Division of Molecular and Cellular Biology, Eunice Kennedy Shriver National Institute of Child Health and Human Development, National Institutes of Health, Bethesda, Maryland, United States of America

<sup>1a</sup> Current address: Dept. of Biochemistry and Structural Biology, University of Texas Health Science Center at San Antonio, San Antonio, Texas, United States of America<sup>2b</sup> Current address: National Institutes of Health, Bethesda, Maryland, United States of America

\* rawal@uthscsa.edu (YR); ahinnebusch@nih.gov, alanh@mail.nih.gov, hinnebusch@mail.nih.gov (AGH)



## OPEN ACCESS

**Citation:** Rawal Y, Qiu H, Hinnebusch AG (2022) Distinct functions of three chromatin remodelers in activator binding and preinitiation complex assembly. PLoS Genet 18(7): e1010277. <https://doi.org/10.1371/journal.pgen.1010277>**Editor:** Gregory S. Barsh, HudsonAlpha Institute for Biotechnology, UNITED STATES**Received:** August 23, 2021**Accepted:** May 28, 2022**Published:** July 6, 2022**Copyright:** This is an open access article, free of all copyright, and may be freely reproduced, distributed, transmitted, modified, built upon, or otherwise used by anyone for any lawful purpose. The work is made available under the [Creative Commons CC0](https://creativecommons.org/licenses/by/4.0/) public domain dedication.**Data Availability Statement:** [S1 File](#) contains (i) annotations of Gcn4 and TBP occupancy peaks listing the coordinates of the Gcn4 occupancy peaks or the windows of  $\pm 100$  bp surrounding the summits of each TBP peak used in plotting heat maps of Gcn4 or TBP occupancies, and (ii) results of MACS2 analysis of uninduced and SM induced TBP ChIP-seq data. A file listing the genomic coordinates of the 250 bp surrounding each tDNA gene is also provided in [S1 File](#). [S2 File](#) contains the data used to construct all plots. Unprocessed and analyzed ChIP-seq data have been deposited in

## Abstract

The nucleosome remodeling complexes (CRs) SWI/SNF, RSC, and Ino80C cooperate in evicting or repositioning nucleosomes to produce nucleosome depleted regions (NDRs) at the promoters of many yeast genes induced by amino acid starvation. We analyzed mutants depleted of the catalytic subunits of these CRs for binding of transcriptional activator Gcn4 and recruitment of TATA-binding protein (TBP) during preinitiation complex (PIC) assembly. RSC and Ino80 were found to enhance Gcn4 binding to both UAS elements in NDRs upstream of promoters and to unconventional binding sites within nucleosome-occupied coding sequences; and SWI/SNF contributes to UAS binding when RSC is depleted. All three CRs are actively recruited by Gcn4 to most UAS elements and appear to enhance Gcn4 binding by reducing nucleosome occupancies at the binding motifs, indicating a positive regulatory loop. SWI/SNF acts unexpectedly in WT cells to prevent excessive Gcn4 binding at many UAS elements, indicating a dual mode of action that is modulated by the presence of RSC. RSC and SWI/SNF collaborate to enhance TBP recruitment at Gcn4 target genes, together with Ino80C, in a manner associated with nucleosome eviction at the TBP binding sites. Cooperation among the CRs in TBP recruitment is also evident at the highly transcribed ribosomal protein genes, while RSC and Ino80C act more broadly than SWI/SNF at the majority of other constitutively expressed genes to stimulate this step in PIC assembly. Our findings indicate a complex interplay among the CRs in evicting promoter nucleosomes to regulate activator binding and stimulate PIC assembly.

## Author summary

ATP-dependent chromatin remodelers (CRs), including SWI/SNF and RSC in budding yeast, are thought to stimulate transcription by repositioning or evicting promoter nucleosomes, and we recently implicated the CR Ino80C in this process as well. The relative importance of these CRs in stimulating activator binding and recruitment of TATA-

the NCBI GEO database under accession number GSE192592.

**Funding:** This work was supported by the Eunice Kennedy Shriver National Institute of Child Health and Human Development, project HD008899-12, of the Intramural Research Program of the National Institutes of Health (AGH). The funders had no role in study design, data collection and analysis, decision to publish, or preparation of the manuscript.

**Competing interests:** The authors have declared that no competing interests exist.

binding protein (TBP) to promoters is incompletely understood. Examining mutants depleted of the catalytic subunits of these CRs, we determined that RSC and Ino80C stimulate binding of transcription factor Gcn4 to nucleosome-depleted regions, or linkers between genic nucleosomes, at multiple target genes activated by Gcn4 in amino acid-starved cells, frequently via evicting nucleosomes from the Gcn4 binding motifs. At some genes, SWI/SNF functionally complements RSC, while opposing RSC at others to limit Gcn4 binding. The CRs in turn are recruited by Gcn4, consistent with a positive feedback loop that enhances Gcn4 binding. The three CRs also cooperate to enhance TBP recruitment, again involving nucleosome depletion, at both Gcn4 target and highly expressed ribosomal protein genes, whereas only RSC and Ino80C act broadly throughout the genome to enhance this key step in preinitiation complex assembly. Our findings illuminate functional cooperation among multiple CRs in regulating activator binding and promoter activation.

## Introduction

In the yeast *Saccharomyces cerevisiae*, most genes transcribed by RNA Polymerase II (Pol II) display a stereotypical pattern of nucleosome organization with a nucleosome-depleted region (NDR) of ~120bp situated upstream of the coding sequences (CDS) and flanked by highly positioned “-1” and “+1” nucleosomes, with the transcription start site (TSS) generally located within the +1 nucleosome. Promoter elements and upstream activation sequences (UAS elements) reside within the NDR and may extend upstream into the -1 nucleosome (-1\_Nuc) [1–4]. The exclusion of nucleosomes from the NDRs can facilitate efficient binding of transcriptional activator proteins at UAS elements [5–7]. The location of the TSS within the +1 nucleosome dictates that the latter is frequently evicted [8,9], or shifted in the 3' direction [10–12], during assembly of the Pol II transcription preinitiation complex (PIC).

Promoter nucleosome organization arises in part from cooperative or antagonistic actions of ATP-dependent chromatin remodeling (CR) complexes [13–14], which are recruited to NDRs or promoter-proximal nucleosomes of many yeast genes [14,15]. The CRs RSC and SWI/SNF generally move the -1 and +1 nucleosomes away from NDRs. RSC has been shown to function in this way at the majority of yeast genes [16–18] to maintain native NDR widths [19,20]. SWI/SNF, in contrast, acts in the promoters of a small fraction of genes that tend to have poor nucleosome phasing and wide NDRs [14,19] and to be highly expressed in WT cells [12]; and SWI/SNF and RSC exhibit functional redundancy at such genes [12,14]. The Ino80 complex (Ino80C) can have opposite effects on nucleosome positioning at different genes, and acts differently from RSC and SWI/SNF at certain genes to move the +1 nucleosome upstream to narrow, rather than widen, the NDR [14,21]. This Ino80C activity is much more pronounced on nuclear depletion of Isw2, catalytic subunit of the CR ISW2; and simultaneous depletion of both Ino80 and Isw2 leads to wider NDRs at a large number of genes and suppresses the widespread narrowing of NDRs conferred by depleting the RSC catalytic subunit Sth1 [14]. There is evidence that Ino80C also “edits” promoter nucleosomes to replace histone variant H2A.Z with conventional H2A [22]; however, there are conflicting findings regarding this activity [23]. Other evidence indicates that Ino80C can function in remodeling conventional nucleosomes containing H2A versus H2A.Z [24–26].

Transcriptional activation of yeast genes is mediated by binding of activator proteins to UAS elements that recruit an array of co-factors to facilitate binding of general transcription factors (GTFs) to the promoter, including TATA-binding protein (TBP), and in recruitment

of Pol II for PIC assembly [3]. In addition to acting as mediators to bridge activators with GTFs or Pol II, co-factors can function to evict or re-position nucleosomes that occlude the promoter or TSS [27]. CRs can function in this way, and inactivation of RSC confers a wide-spread reduction in expression of many genes [16], particularly those with intermediate to low expression levels in WT cells [28]. RSC, in cooperation with general regulatory factors (GRFs) Reb1, Abf1 and Rap1, appears to slide the +1 nucleosome downstream to enhance TBP binding to the promoters of many genes [29]. SWI/SNF partners with RSC [12] and histone acetyltransferase Gcn5 [30] in stimulating transcription of many highly transcribed, constitutively expressed genes. SWI/SNF was also implicated in transcriptional activation of condition-regulated genes such as *PHO5* [31], *SUC2* [32], *RNR1* [33], various genes involved in metabolic reprogramming [11], and genes activated by heat-shock [34] or amino acid starvation [12]. For many genes in this last group, mostly induced by transcriptional activator Gcn4, SWI/SNF partners with RSC to evict promoter nucleosomes and reposition the remaining -1 and +1 nucleosomes to widen the NDRs and promote transcription [12]. There is evidence that downstream repositioning of the +1 nucleosome by SWI/SNF enhances TBP binding to the promoters at a subset of SWI/SNF-dependent genes [14].

Ino80C is required for efficient transcriptional activation of genes induced in response to inositol depletion [14], and it partners with SWI/SNF and RSC in nucleosome remodeling during induction of the *PHO5* gene [31,35] and at a subset of genes induced by amino acid starvation [26]. For the latter, Ino80C promotes eviction of promoter nucleosomes and appears to stimulate transcription by enhancing TBP recruitment. Ino80C is also critical for expression of TORC1-responsive genes during the yeast metabolic cycle (YMC) and thus helps to coordinate respiration and cell division with periodic gene expression [36]. The frequent downstream repositioning of the +1 nucleosome on co-depletion of Ino80 and ISW2 mentioned above is associated with enhanced TBP binding and elevated transcription, often involving cryptic TSSs normally occluded by the +1 nucleosome [14]. There is also evidence that Ino80 acts to restore, rather than remove, promoter nucleosomes following their rapid eviction in response to osmotic stress, and thereby prevent prolonged transcriptional activation of certain stress-induced genes [37]. Another study indicates that Ino80C is recruited by TBP to both promoters and terminators of Pol II genes, in association with TBP-binding factors Mot1 and NC2, where they act to suppress cryptic promoters in intergenic regions and also some physiological promoters at transcriptionally inactive genes [38].

While there is evidence that CRs influence transcriptional activation by evicting or displacing promoter nucleosomes to control access of GTFs and attendant PIC assembly, much less is known about their importance in regulating the binding of transcriptional activators to the UAS elements of yeast genes. In vitro evidence from single-molecule analysis indicates that RSC promotes binding of transcriptional activator Ace1 to the *CUP1* promoter by increasing accessibility of the Ace1 binding site in chromatin to reduce the search time for Ace1 binding [39]. SWI/SNF remodeling activity is critical for efficient binding of activator Pho4 at the *PHO5* UAS [40]. On the other hand, in vitro single-molecule studies indicate that SWI/SNF can impede binding of the Gal4 DNA binding domain by sliding a nucleosome across its binding site [41]. Moreover, human SWI/SNF was shown in vitro to displace the glucocorticoid receptor from its binding site in a reconstituted nucleosome array, likely contributing to the transient nature of GR interactions with the promoter in chromatin [42]. Thus, it seems that SWI/SNF can either enhance or impede activator binding in different settings.

Depriving yeast cells of an amino acid, including starvation for isoleucine and valine, achieved with the inhibitor sulfometuron methyl (SM), increases the transcription of hundreds of genes, most of which are dependent on activator Gcn4 for induction [43–45]. Previously, by ChIP-Seq analysis of Pol II subunit Rpb3, we identified a group of ca. 200 genes exhibiting

$\geq 2$ -fold induction of Pol II occupancies averaged across the CDS on SM treatment. Parallel ChIP-Seq analysis of histone H3 revealed a marked eviction of nucleosomes in the promoter intervals spanning the -1 and +1 nucleosomes and intervening NDRs at 70 of these SM-induced genes, and lesser increases in H3 occupancies at the remaining 134 induced genes [30]. As noted above, examining mutants lacking the catalytic subunits of SWI/SNF (*snf2 $\Delta$* ) or Ino80C (*ino80 $\Delta$* ), or conditionally depleted of the essential catalytic subunit of RSC by transcriptional shut-off (*P<sub>TET</sub>-STH1*), revealed overlapping roles for these three CRs in evicting promoter nucleosomes and inducing transcription of SM-induced genes [12,26,30]. Here, we set out to examine their roles in binding of Gcn4 to UAS elements, which increases sharply on translational induction of Gcn4 protein by SM [46].

Interestingly, our previous ChIP-seq analysis of Gcn4 in SM-treated WT cells revealed that only ~40% of the 546 sites of induced binding detected throughout the genome are located upstream of genes (5' sites), with the majority occurring instead within the CDS (ORF sites). Roughly 70% of the genes with conventional 5' sites show evidence of transcriptional activation in amino acid starved cells and are likely direct targets of Gcn4, whereas only ~20% of the genes with only ORF binding sites are transcriptionally activated. Mutation of the internal Gcn4 binding sites at a number of the latter genes was shown to impair their transcriptional activation by SM, demonstrating that Gcn4 can activate 5'-positioned promoters by binding within the downstream ORFs. Gcn4 binding to the majority of 5' sites occurs within NDRs; while the binding at ORF sites generally occurs within linkers between genic nucleosomes. Moreover, only ~30% of all predicted Gcn4 binding motifs in the genome are occupied by Gcn4 in SM-induced cells, and the two most important features of bound motifs are (i) a strong match to the consensus Gcn4 motif and (ii) lower than average nucleosome occupancy [46]. These findings suggest that Gcn4 binding is inefficient when its binding motif maps within a nucleosome, in agreement with previous findings that Gcn4 binding to the *HIS4* UAS is enhanced by Rap1 and its ability to exclude nucleosomes [5,6]. Nucleosome occupancy is also a key determinant of binding by activator Leu3 in the yeast genome [47]. Recent results indicating cooperation between different GRFs and RSC in downstream positioning of the +1 nucleosome for NDR formation [29], led us to wonder whether Gcn4 binding to 5' sites at many UASs might be stimulated by RSC.

The results of the current study indicate that Gcn4 binding at many 5' sites, as well as ORF sites, is stimulated by RSC, by SWI/SNF in cells depleted of RSC, and by Ino80C. Surprisingly, when RSC is present, SWI/SNF acts primarily to limit rather than enhance Gcn4 occupancies at 5' sites, suggesting a dual role for SWI/SNF in activator binding. We found that Gcn4 recruits all three CRs to 5' sites, consistent with their direct roles, and indicating feedback loops that regulate Gcn4 binding at UAS elements. Other evidence indicates that the CRs enhance Gcn4 binding by reducing nucleosome occupancies of the Gcn4 binding motifs, supporting the notion that Gcn4 binding is impeded by nucleosomes. Examining the effects of deleting/depleting the CRs on TBP occupancies showed that RSC and SWI/SNF collaborate to enhance TBP recruitment at Gcn4 target genes, as does Ino80C, in a manner associated with nucleosome eviction at the TBP binding sites. Cooperation among the CRs is also evident at the highly transcribed ribosomal protein genes (RPGs), while RSC and Ino80C act more broadly than SWI/SNF to stimulate this step in PIC assembly throughout the rest of the genome.

## Results

### RSC, SWI/SNF and Ino80C modulate Gcn4 binding within NDRs and coding regions

Our previous ChIP-seq analysis of Gcn4 in SM-induced WT cells identified 117 Gcn4 binding sites located 5' of an annotated TSS in the canonical location of yeast UAS elements, which

appear to mediate transcriptional activation of the adjacent genes during amino acid starvation (5' Gcn4 peaks). An additional 62 Gcn4 peaks were identified within coding sequences that appear to activate transcription of the full-length transcript of the corresponding gene or an adjacent gene lacking a Gcn4 peak (ORF peaks) [46]. As reported previously [46], averaging the Gcn4 occupancies measured by ChIP-seq over the 5' or ORF peaks and aligning them to the Gcn4 binding motifs reveals that Gcn4 occupancies are highly induced by SM in WT cells, and that the summits of the occupancy peaks coincide precisely with the Gcn4 binding motifs (Fig 1A(i) and 1B(i), yellow vs. blue).

Our previous ChIP-seq analysis of histone H3 using chromatin fragmented by micrococcal nuclease digestion, which preferentially cuts within linkers, allowed us to estimate the positions of nucleosome dyads from the midpoints of immunoprecipitated DNA fragments. Averaging dyad densities over all 5' or ORF peaks reveals that Gcn4 binding motifs of 5' sites are generally located in the centers of NDRs, whereas the motifs for ORF peaks reside in the linkers between the genic nucleosomes observed in untreated WT cells (Fig 1E and 1F, red tracings). The dyad densities of the -1 and +1 nucleosomes and the intervening NDRs at the 5' Gcn4 peaks are diminished, and the NDRs become wider, in response to SM treatment (Fig 1E, blue vs. red), reflecting eviction and repositioning of the -1 and +1 nucleosomes [12]. The dyad densities of the genic nucleosomes flanking ORF peaks are also diminished; however, the spacing between them appears unaltered by SM treatment (Fig 1F, blue vs. red). The fact that Gcn4 binds preferentially to motifs located outside of nucleosomes, and our previous findings that eviction or repositioning of promoter nucleosomes induced by SM treatment involves SWI/SNF, RSC and Ino80C [12,26], led us to examine whether Gcn4 binding is enhanced by one or more of these CRs.

To this end, we conducted Gcn4 ChIP-seq analysis on *snf2Δ* and *ino80Δ* mutants, lacking the catalytic subunits of SWI/SNF or Ino80C, respectively, and on a  $P_{TET}$ -*STH1* strain in which the RSC catalytic subunit was transcriptionally repressed by addition of doxycycline (Dox) for 8h, in cells treated with SM to induce Gcn4. We similarly examined a *snf2Δ*  $P_{TET}$ -*STH1* double mutant treated with Dox to examine the effects of depleting RSC in cells lacking SWI/SNF. We observed a slight reduction in the averaged Gcn4 occupancies for the group of 5' sites on depleting Sth1 in  $P_{TET}$ -*STH1* versus WT cells under inducing conditions ( $P_{TET}$ -*STH1*\_I vs. WT\_I), but a more substantial reduction of ~50% in the induced *snf2Δ*  $P_{TET}$ -*STH1* double mutant versus WT\_I cells (Fig 1A(i), red & cyan vs. yellow). Surprisingly, in the *snf2Δ* single mutant, the averaged Gcn4 occupancy was markedly increased compared to WT cells (Fig 1A(i), grey vs. yellow). Calculating the mean Gcn4 occupancy per nucleotide across each 5' site (with boundaries defined as described in Materials and Methods), revealed a significant reduction in median Gcn4 occupancy in *snf2Δ*  $P_{TET}$ -*STH1*\_I cells, but an increased median occupancy in *snf2Δ*\_I cells, compared to WT\_I cells (Fig 1C(i), cols. 5 & 3 vs. 2). These opposite effects on median Gcn4 occupancies conferred by *snf2Δ* (increased binding) versus the *snf2Δ*  $P_{TET}$ -*STH1* double mutant (decreased Gcn4 binding) are evident in comparing the results obtained from the individual biological replicates for these two mutants and WT\_I cells (S1A Fig, grey or cyan vs. yellow), which were combined to generate the composite results in Fig 1C. High reproducibility of results from biological replicates is also illustrated for six representative genes with 5' Gcn4 sites in S2A–S2C Fig. The ORF Gcn4 peaks also showed reductions in  $P_{TET}$ -*STH1*\_I and *snf2Δ*  $P_{TET}$ -*STH1*\_I cells, but no significant increase in *snf2Δ*\_I cells (Fig 1B(i) and 1D(i)). Similar analyses showed that the *ino80Δ* mutation conferred moderate reductions in both average and median Gcn4 occupancies at the 5' sites (Fig 1A(ii) and 1C(ii), gold vs. yellow), which is less severe than that just described for the *snf2Δ*  $P_{TET}$ -*STH1* double mutant. The *ino80Δ* mutation also reduced Gcn4 occupancies at ORF peaks (Fig 1B(ii) and 1D(ii)), to an extent comparable to that shown above for the  $P_{TET}$ -*STH1*\_I single mutation (Fig 1B(i) and 1D(i)).

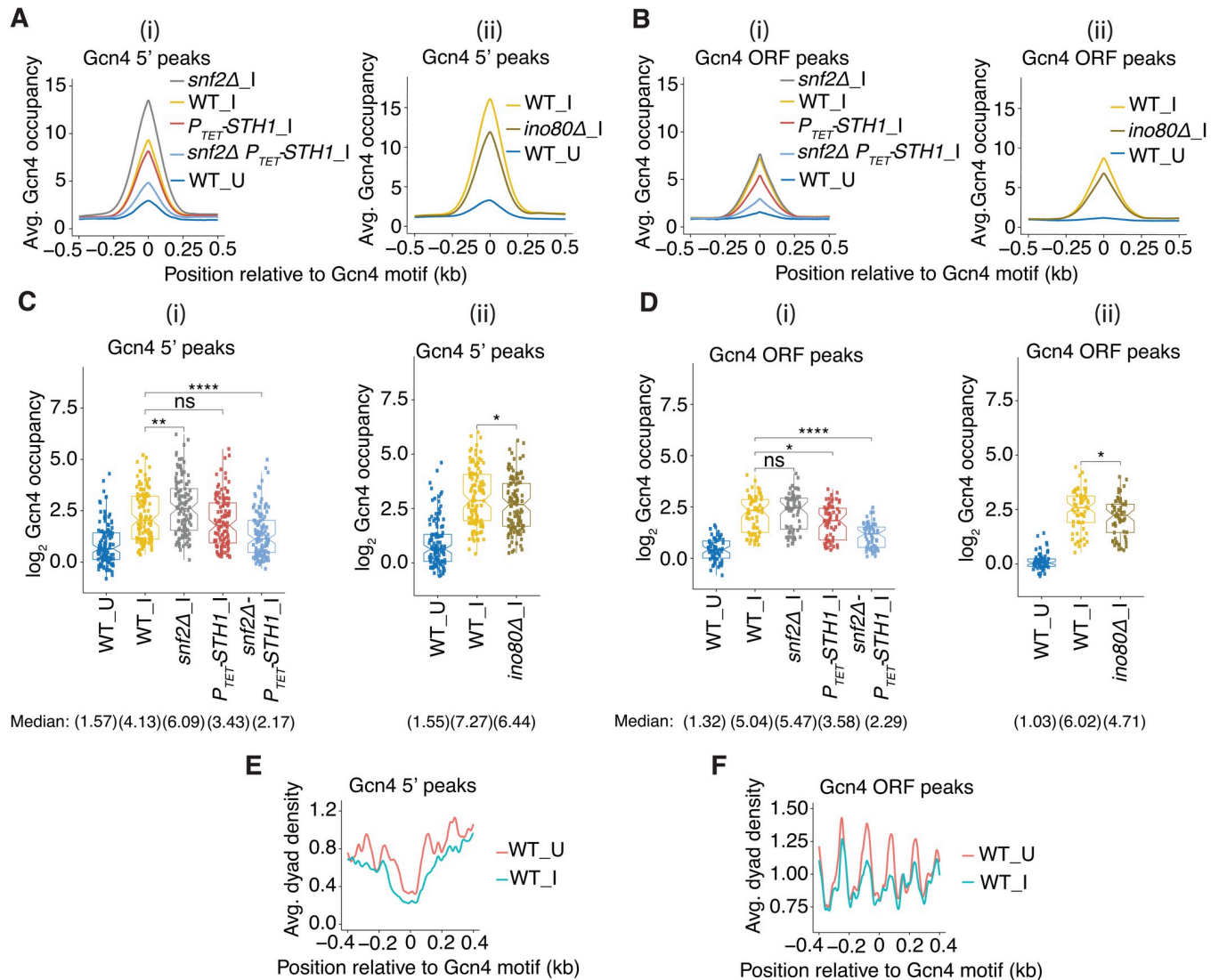


**Fig 1. Gcn4 occupancy changes in CR mutants.** (A–B) Gcn4 occupancies at each base pair surrounding the consensus binding motifs averaged over (A) all 117 5' sites or (B) all 62 ORF Gcn4 peaks in WT\_U (blue), WT\_I (yellow), and SM-induced CR mutants for (i) *snf2Δ*\_I (gray), *P<sub>TET</sub>-STH1*\_I (red), *snf2Δ P<sub>TET</sub>-STH1*\_I (cyan); and (ii) WT\_I (yellow) and *ino80Δ*\_I (gold). In these and all similar plots below, yeast strain/condition labels adjacent to the tracings are listed in decreasing order of summit heights. (C–D) Notched box plots of log<sub>2</sub> Gcn4 occupancies per nucleotide averaged over the peak coordinates assigned by MACS2 analysis of (C) 5' and (D) ORF Gcn4 peaks for (i) WT\_U, WT\_I, and CR mutants *snf2Δ*\_I, *P<sub>TET</sub>-STH1*\_I and *snf2Δ P<sub>TET</sub>-STH1*\_I; and (ii) WT\_U, WT\_I, and *ino80Δ*\_I samples, color-coded as in (A–B). For these and all subsequent box plots, each box depicts the interquartile range containing 50% of the data, intersected by the median; the notch indicates a 95% confidence interval (CI) around the median, and *p* values for the significance of differences in median values calculated by the Mann-Whitney-Wilcoxon test are indicated as follows: \*\*\*\*,  $\leq 0.0001$ ; \*\*\*,  $\leq 0.001$ ; \*\*,  $\leq 0.01$ ; \*,  $\leq 0.05$ ; ns,  $> 0.05$ . Unlogged median Gcn4 occupancies are indicated under the respective strain labels. Data analyzed in (A–D) were calculated from Gcn4 ChIP-seq analysis of sonicated chromatin from 2–4 biological replicates and normalized to the average occupancy per nucleotide on each chromosome for each data set. (E–F) Average dyad densities calculated from H3 MNase-ChIP-seq data aligned to the Gcn4 consensus motifs for (E) 5' and (F) ORF Gcn4 peaks in WT cells either untreated (\_U) or SM-treated (\_I). Midpoints (dyads) of nucleosome-size sequences between 125 and 175 bp were mapped with respect to Gcn4 consensus motifs. Average profiles were smoothed using a moving average filter with a span of 31 bp. The data were normalized to the average occupancy per nucleotide on each chromosome for each data set.

<https://doi.org/10.1371/journal.pgen.1010277.g001>

To explore further the contributions of the CRs at individual Gcn4 motifs, we sorted the 5' Gcn4 peaks according to their reductions in Gcn4 occupancies in the *snf2Δ P<sub>TET</sub>-STH1*\_I double mutant compared to WT\_I cells. A heat map showing the differences in Gcn4 occupancies between the double mutant and WT for this ordering of 5' sites is shown in Fig 2A(i), which

was calculated from the corresponding occupancies for these two strains displayed in the heat maps of Fig 2B(i)-(ii). Thus, the Gcn4 5' sites in the top quartile of the maps (designated Set\_1 in Fig 2B) exhibit the greatest occupancy reductions in the double mutant versus WT cells, as indicated by the darkest blue hues in the difference map of Fig 2A(i). Similar difference maps were generated for the  $P_{TET}$ -*STH1* or *snf2Δ* single mutants, shown in Fig 2A(ii)-(iii), based on the Gcn4 occupancies measured in these strains displayed in Fig 2B(iii)-(iv). The Set\_1 peaks display relatively smaller occupancy decreases in the  $P_{TET}$ -*STH1*\_I single mutant vs. WT\_I than observed in the double mutant (lighter blue hues in the difference map of Fig 2A(ii) vs. Fig 2A(i) for the top quartile). In *snf2Δ*\_I cells, the Set\_1 peaks variously show small decreases, no change, or small increases in Gcn4 occupancy compared to WT\_I cells (Fig 2A(iii), top quartile). The Gcn4 peaks in the middle two quartiles of the maps (dubbed Set\_2 in Fig 2B) show strong to moderate reductions in the double mutant, lesser reductions in the  $P_{TET}$ -*STH1*\_I single mutant, but generally increased occupancies in *snf2Δ*\_I cells versus WT\_I cells (Fig 2A(i)-(iii), middle quartiles). The genes in the bottom quartile of the maps (Set\_3) tend to show similar, small occupancy increases or decreases in both the double and single  $P_{TET}$ -*STH1*\_I mutants (Fig 2A(i)-(ii)), while showing marked increases in Gcn4 occupancies in *snf2Δ*\_I cells (Fig 2A(iii)).

The trends depicted in the heat maps of Fig 2A and 2B were confirmed by quantifying the Gcn4\_I occupancies in each peak and calculating the median values for the three sets of peaks. As expected, Set\_1 displays a greater reduction in Gcn4 median occupancy in the double mutant versus the  $P_{TET}$ -*STH1*\_I single mutant, but no significant change in the *snf2Δ* single mutant (Fig 2C(i), cols. 3–5 vs. 2). Set\_2 also shows a greater reduction in median occupancy in the double mutant versus the  $P_{TET}$ -*STH1*\_I single mutant, even though Gcn4 occupancy is significantly elevated in the *snf2Δ* single mutant containing WT *STH1* (Fig 2C(ii), cols. 3–5 vs. 2). Set\_3 shows no significant decrease in median Gcn4 occupancy in either of the  $P_{TET}$ -*STH1*\_I mutants, but increased occupancies in the *snf2Δ* single mutant (Fig 2C(iii), cols. 3–5 vs. 2). The differential effects of the *snf2Δ* and  $P_{TET}$ -*STH1* mutations on Gcn4 binding in the three sets of 5' sites summarized in Fig 2C are also evident for the biological replicates for each of the mutants (S1B Fig), including increased Gcn4 binding in both *snf2Δ* replicates for Set\_3 but not for Set\_1 sites (grey vs. yellow), and decreased Gcn4 binding in all three replicates of the *snf2Δ* $P_{TET}$ -*STH1* double mutant for Set\_1 but not for Set\_3 sites (cyan vs. yellow).

The results in Fig 2A–2C were analyzed further in S3 Fig by plotting the changes in Gcn4 occupancies at each 5' site between WT and mutant cells. For Set\_1 and Set\_2, most peaks show moderate reductions in Gcn4 occupancies in  $P_{TET}$ -*STH1*\_I versus WT\_I cells (S3A Fig, Sets \_1, \_2), which are exacerbated by deletion of *SNF2* in the double mutant compared to the  $P_{TET}$ -*STH1* single mutant (S3B Fig, Sets \_1, \_2). The Set\_3 peaks exhibit variable occupancy changes in both the  $P_{TET}$ -*STH1* single and double mutant versus WT (S3A and S3B Fig, Set\_3). In contrast, the *snf2Δ* single mutation confers variable changes for Set\_1 sites, but moderate or strong increases in Gcn4 occupancies for Set\_2 and Set\_3 sites, respectively (S3C Fig).

Finally, we constructed a sectorized scatterplot of the changes in Gcn4 binding conferred by *snf2Δ* versus the *snf2Δ*  $P_{TET}$ -*STH1* double mutation, color-coded according to Set\_1, \_2, or \_3 sites. Although the changes are significantly correlated for all 5' sites ( $R = 0.64$ ,  $P < 1.2 \times 10^{-14}$ ), nearly all of the points fall into the upper left quadrant indicating that decreases in binding in the double mutant are generally associated with increased Gcn4 binding in the *snf2Δ* single mutant (S3D Fig). Moreover, the group of Set\_3 sites (blue points) show the largest increases in Gcn4 binding in *snf2Δ* cells but the smallest reductions in the double mutant; whereas the Set\_1 sites (red points) show the largest decreases in Gcn4 binding in the *snf2Δ*  $P_{TET}$ -*STH1* double mutant but the smallest increases in the *snf2Δ* single mutant (S3D Fig). These insights confirm those reached from the orthogonal analyses described above (Figs 2A–

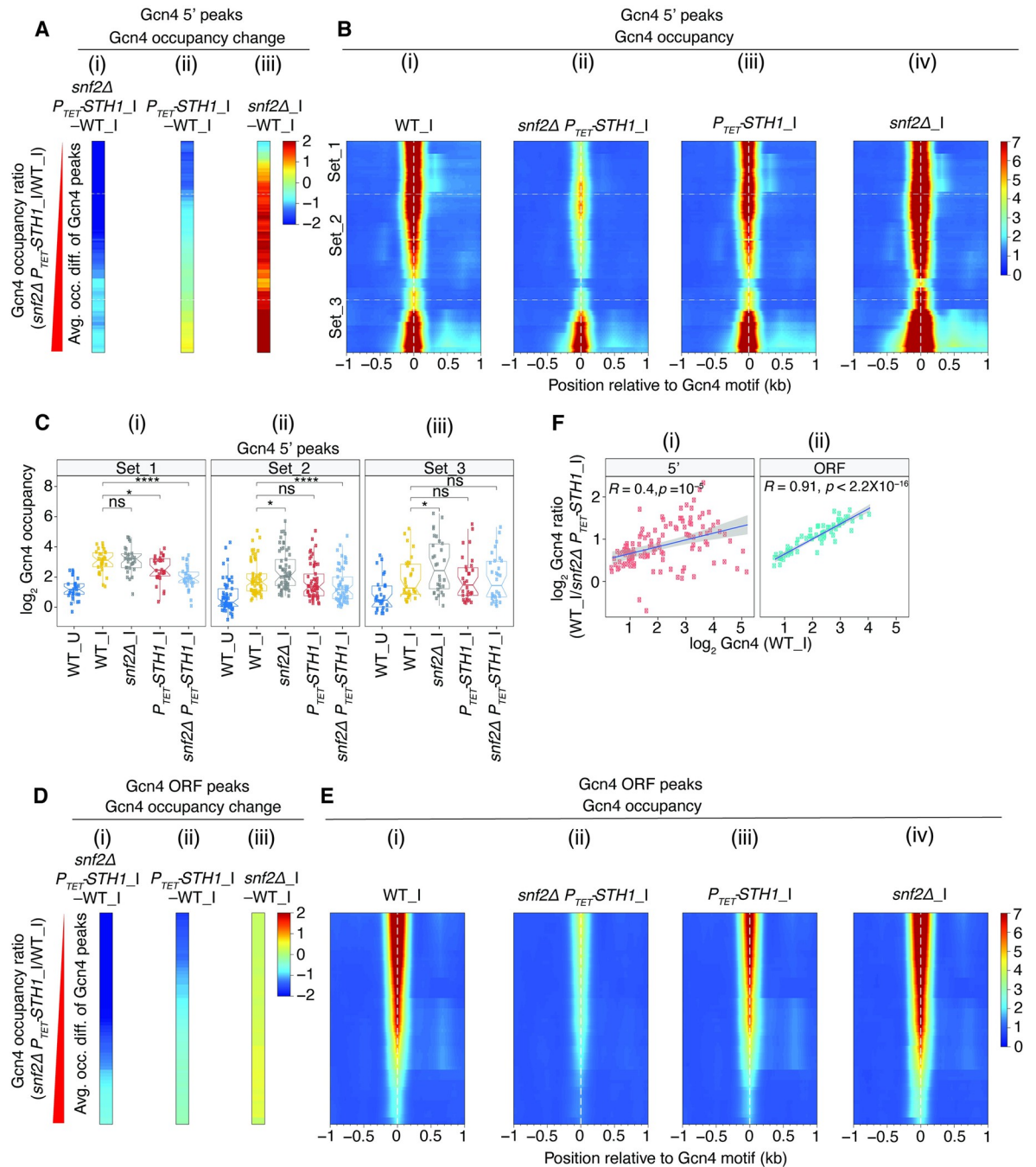


**Fig 2. SWI/SNF and RSC have opposing effects on Gcn4 binding at 5' sites.** (A) Heat maps of differences in Gcn4 occupancies averaged across the coordinates of 5' sites between the indicated mutant and WT\_I samples for (i) *snf2Δ P<sub>TET</sub>-STH1\_I*, (ii) *P<sub>TET</sub>-STH1\_I* and (iii) *snf2Δ\_I* cells. Gcn4 5' sites were sorted by increasing order of the ratio of Gcn4 occupancies in the double mutant *snf2Δ P<sub>TET</sub>-STH1\_I* vs. WT\_I. The peaks belonging to the first (Set\_1, n = 30), middle two (Set\_2, n = 57) and fourth (Set\_3, n = 30) quartiles of fold-changes are arranged from top to bottom and separated by white lines across the maps. In these and all heat maps below, color-coding of values in the heat maps are shown in a key to the right of the map(s). (B) Heat map depictions of Gcn4 occupancies surrounding the Gcn4 motifs of 5' sites in (i) WT\_I, (ii) *snf2Δ P<sub>TET</sub>-STH1\_I*, (iii) *P<sub>TET</sub>-STH1\_I*, and (iv) *snf2Δ\_I* cells, for the same ordering of 5' sites as in (A). The locations of 5' Gcn4 peaks in Sets\_1 to 3 are indicated. (C) Notched box plots of log<sub>2</sub> Gcn4 occupancies in WT\_U, WT\_I, or *snf2Δ\_I*, *P<sub>TET</sub>-STH1\_I* and *snf2Δ P<sub>TET</sub>-STH1\_I* cells in 3 sets of Gcn4 5' sites comprised of the (i) first (Set\_1, n = 30), (ii) middle two (Set\_2, n = 57) and (iii) last (Set\_3, n = 30) quartiles of the fold-changes in *snf2Δ P<sub>TET</sub>-STH1\_I* vs. WT\_I cells as depicted in Fig 2B(i). (D & E) Same analyses shown in (A & B) except for Gcn4 ORF peaks. (F) Scatterplot of log<sub>2</sub> ratios of Gcn4 occupancy changes in WT\_I vs. *snf2Δ P<sub>TET</sub>-STH1\_I* plotted against log<sub>2</sub> Gcn4 occupancies in WT\_I cells for (i) 5' (left panel) and (ii) ORF (right) Gcn4 peaks. Pearson correlation coefficients (R) and associated p values are indicated.

<https://doi.org/10.1371/journal.pgen.1010277.g002>



2C and S3A–S3C); moreover, the segregation of data points into three clusters of different colors in S3D Fig justifies the utility of dividing the 5' sites into Set\_1, \_2, and \_3 for downstream analysis.

Together, these findings indicate that RSC enhances Gcn4 binding for Set\_1 and Set\_2 sites, with a greater contribution for Set\_1, but has weak and variable effects on Set\_3 sites. In WT cells, SWI/SNF generally inhibits, rather than promotes, Gcn4 binding at the Set\_2 and \_3 sites, with the greatest inhibition for the Set\_3 sites that are largely insensitive to RSC, while SWI/SNF has variable effects on the Set\_1 sites most dependent on RSC. In cells depleted of RSC, however, SWI/SNF promotes rather than inhibits binding at 5' sites in Set\_1 and \_2, thus compensating for reduced RSC function at the peaks most dependent on RSC; and SWI/SNF no longer inhibits Gcn4 binding to most peaks in Set\_3. One way to explain these last findings for Set\_3 would be to propose that the inhibitory effect of SWI/SNF on Gcn4 binding is offset by the stimulatory role that SWI/SNF exerts upon depletion of Sth1, with little net change in Gcn4 occupancy found in the double mutant. Differential effects of the  $P_{TET}$ -*STH1*\_I and *snf2Δ* mutations on Gcn4 occupancies for the three Sets of 5' sites described above are illustrated for two archetypal members of each Set in S4A–S4C ((i)-(ii)) Fig.

It is worth noting that we previously obtained results fully consistent with those reported here by ChIP analysis of Gcn4 for particular genes, where occupancies were calculated as the ratios of input DNA recovered in the immunoprecipitates (determined by PCR analysis) and corrected for the corresponding ratios observed for a non-transcribed sequence on chromosome V [30]. Thus, as summarized in S3A Table, we reported that Gcn4 occupancy was elevated in *snf2Δ* versus WT cells by 2.1- and 1.6- fold in the UASs of Set\_3 genes *ARG1* and *ARG4*, respectively, elevated by 1.5-fold at the UAS of Set\_2 gene *CPA2*, and did not increase at the Set\_1 gene *HIS4*, in agreement with the ChIP-Seq analysis of *ARG1* and *HIS4* shown in S4C(i) and S4A(i) Fig. Extending the PCR-ChIP analysis further to include the  $P_{TET}$ -*STH1* and *snf2Δ*  $P_{TET}$ -*STH1* mutants, we observed a marked decrease in Gcn4 binding at the Set\_1 gene *HIS4* only in the double mutant, and no decrease in either mutant for the Set\_3 gene *ARG1* (S3B Table), again consistent with our Gcn4 ChIP-seq results in S4A(i) and S4C(i) Fig.

The effects of the CR mutations on Gcn4 occupancies at binding sites in coding regions were less complex, as the majority of Gcn4 ORF peaks show relatively strong reductions in the *snf2Δ*  $P_{TET}$ -*STH1* double mutant, moderate reductions in the  $P_{TET}$ -*STH1*\_I single mutant, and little change in the *snf2Δ*\_I single mutant (see difference maps in Fig 2D(i)-(iii), based on the heat maps in Fig 2E(i)-(iv)). Thus, as noted above for 5' Gcn4 peaks, RSC generally stimulates Gcn4 binding and SWI/SNF partially compensates for RSC function on depletion of RSC, but there is no evidence for an inhibitory effect of SWI/SNF, on Gcn4 binding at the ORF peaks. Interestingly, the magnitude of the reduction in Gcn4 occupancy at the ORF peaks in the *snf2Δ*  $P_{TET}$ -*STH1* double mutant versus WT cells is strongly correlated with Gcn4 occupancy at these peaks in WT\_I cells (Fig 2F(ii)), suggesting an increasing requirement for RSC or SWI/SNF as the occupancy at ORF sites increases. A significant but considerably weaker correlation exists for 5' Gcn4 peaks (Fig 2F(i)), possibly reflecting the more complex interplay between RSC and SWI/SNF at the 5' sites.

Analyzing the effects of *ino80Δ* for the same ordering of 5' Gcn4 peaks described above reveals that the 5' sites in Set\_1 show reductions of lesser magnitude compared to those given by *snf2Δ*  $P_{TET}$ -*STH1*; whereas comparable, smaller reductions are conferred by *ino80Δ* and *snf2Δ*  $P_{TET}$ -*STH1* for Set\_2 sites (S5A(i) vs. (ii) Fig and S5B(i)-(iv) Fig, Sets\_1, \_2). In contrast, many of the Set\_3 sites display greater reductions in Gcn4 occupancies in *ino80Δ* cells versus *snf2Δ*  $P_{TET}$ -*STH1* cells (S5A(i) vs. (ii) Fig and S5B(i)-(iv) Fig, Set\_3), suggesting a greater dependence on Ino80C compared to RSC for this group. For the ORF Gcn4 peaks, *ino80Δ* confers a moderate reduction in Gcn4 binding across the spectrum of binding sites, much less

than conferred by *snf2Δ P<sub>TET</sub>-STH1* (S5C(i) vs. (ii) Fig and S5D (i)-(iv) Fig), but similar to that shown in Fig 2D(ii) for the *P<sub>TET</sub>-STH1* single mutation.

To identify all 5' sites with a heightened dependence on Ino80C, we ordered them differently based on their decreased Gcn4 occupancies in *ino80Δ* \_I versus WT\_I cells, generating heat maps with peaks exhibiting the largest occupancy reductions conferred by *ino80Δ* at the top of the maps (S6A (i)-(iii) Fig). As expected for this ordering, *ino80Δ* substantially decreases the median occupancy for the top quartile of peaks (designated Set\_I), but not for the lower quartiles in Sets \_II or \_III (S6C(i)-(iii) Fig). The corresponding difference maps for the *P<sub>TET</sub>-STH1* and *snf2Δ P<sub>TET</sub>-STH1* mutations for this same ordering of 5' sites reveals more uniform reductions in Gcn4 occupancies across the sites compared to those given by *ino80Δ* (S6B(i)-(ii) vs. S6A(i) Fig); and the *snf2Δ* single mutation generally confers increased Gcn4 occupancies for sites in Sets \_I, and \_II that show decreased occupancies in *ino80Δ* \_I versus WT\_I cells (S6B(iii) vs. S6A(i) Fig). Thus, certain 5' sites have a particularly strong dependence on Ino80C, but little requirement for RSC or SWI/SNF in Gcn4 binding in WT cells. The importance of Ino80C for WT Gcn4 binding is illustrated for the *YHR162W* and *HIS4* genes in S12E (i)-(ii) Fig (rows 2–3).

We considered the possibility that the changes in Gcn4 occupancies in the mutants described above involve changes in Gcn4 expression. Quantifying the occupancies of Pol II across the *GCN4* coding sequences from our previous ChIP-seq analysis of Rpb3 indicated similar reductions in *GCN4* transcription of ~32–37% in the induced *snf2Δ P<sub>TET</sub>-STH1* and *P<sub>TET</sub>-STH1* mutants, but no change in *snf2Δ* \_I or *ino80Δ* \_I cells [12,26] (summarized in S7A Fig, cols. 3–6 vs. 2). Similarly, our Western analyses of Gcn4 protein levels indicated comparable reductions of ~20% in the *P<sub>TET</sub>-STH1* and *snf2Δ P<sub>TET</sub>-STH1* mutants, but no change conferred by *snf2Δ* [12] (S7B Fig) or by *ino80Δ* [26]. The fact that the *snf2Δ P<sub>TET</sub>-STH1* and *P<sub>TET</sub>-STH1* mutations confer similar, moderate reductions in Gcn4 expression (S7A and S7B Fig) suggests that the considerably larger reductions in Gcn4 occupancies at most 5' sites observed for *snf2Δ P<sub>TET</sub>-STH1* \_I versus *P<sub>TET</sub>-STH1* \_I cells (Fig 1A and 1C and Fig 2A–2C) do not result from decreased Gcn4 abundance.

To examine this last issue further, we reasoned that if reduced Gcn4 occupancies arise primarily from reduced Gcn4 abundance, then the occupancy reductions should occur preferentially at binding sites of lower affinity or accessibility in chromatin. We showed previously that Gcn4 occupancies in WT cells are dictated primarily by their match to the consensus motif, with a secondary contribution from the distance of the motif from the dyad of the nearest nucleosome [46]. Consistent with this, Gcn4 occupancies in WT\_I cells are positively correlated with the match of the binding motif to the consensus sequence (quantified as “Find Individual Motif Occurrences” (FIMO) scores) for both 5' and ORF peaks of Gcn4 occupancies (S7C and S7D Fig). Accordingly, we used Gcn4 occupancies in WT\_I cells as a proxy for affinity/accessibility of the binding motifs in chromatin. As shown above in Fig 2C, the 5' Gcn4 peaks in Set\_1, showing the largest occupancy reductions in *snf2Δ P<sub>TET</sub>-STH1* \_I cells, have WT\_I Gcn4 occupancies considerably greater than those in Set\_2 and Set\_3, which exhibit smaller reductions in binding in the double mutant (Fig 2C(i) vs. (ii)-(iii), yellow data). Consistent with this, and also noted above, the reductions in Gcn4 binding in the double mutant are positively correlated with WT\_I Gcn4 occupancies for both the 5' and ORF peaks (Fig 2F (i)-(ii)). Moreover, the 5' sites in Set\_1 have higher median FIMO scores than those in Set\_2 or \_3 (S7E Fig). These findings indicating that Gcn4 sites of highest occupancy/affinity tend to show the largest occupancy decreases in the *snf2Δ P<sub>TET</sub>-STH1* mutant do not support the possibility that the reductions in Gcn4 abundance are important drivers of diminished Gcn4 occupancy in this mutant. The tendency for Gcn4 peaks with greater occupancies in WT to show larger binding reductions is also evident for the *ino80Δ* mutant, for both 5' and ORF

peaks (S6D(i)-(ii) Fig). Because *ino80Δ* does not alter *GCN4* transcription (S7A Fig) or Gcn4 protein abundance [26], it appears that intrinsic properties of high-occupancy Gcn4 binding sites render them relatively more dependent on CR function for robust Gcn4 binding.

### Evidence that SWI/SNF, RSC, and Ino80C are recruited by Gcn4 to NDRs and act directly to regulate Gcn4 binding

To provide evidence that SWI/SNF, RSC and Ino80C function directly at Gcn4 motifs to regulate Gcn4 binding, we examined whether these CRs are recruited to Gcn4 binding sites. To this end, we conducted ChIP-seq analysis of the Myc epitope-tagged catalytic subunits, Snf2, Sth1, and Ino80, and corrected the occupancies for those obtained from ChIP-seq of an isogenic untagged strain. Heatmaps of the corrected CR occupancies sorted by the WT\_I Gcn4 occupancies revealed that Snf2-myc occupancies are generally centered on the Gcn4 binding motifs, and that they tend to increase with increasing Gcn4 binding (Fig 3A(i)), yielding a direct correlation between Snf2-myc\_I and Gcn4\_I occupancies (Fig 3B(i)). A precise coincidence in the occupancies of Gcn4 and Snf2-myc is evident for several 5' Gcn4 peaks associated with particularly high induced Snf2-myc occupancies (S8A–S8E Fig). There is also evidence, however, that Snf2-myc occupancy is greatest upstream of the Gcn4 motif at a subset of 5' sites (Fig 3A(i)), which might indicate interaction of SWI/SNF with another transcription factor bound at these promoters instead of Gcn4. The Sth1-myc occupancies are also generally centered on the Gcn4 motifs, but they are lower overall (Fig 3A(ii)), and the correlation between Gcn4 and Sth1-myc occupancies is less pronounced (Fig 3B(ii)); however, Snf2-myc and Sth1-myc occupancies at the 5' Gcn4 peaks are positively correlated (S9A(i) Fig). Ino80-myc occupancies also peak at, or somewhat upstream, of the Gcn4 motifs at most 5' sites, and show a positive correlation with WT\_I Gcn4 occupancies (Fig 3B(iii)); although they are higher than expected at the 5' sites of lowest Gcn4 occupancies found at the bottom of the heat map in Fig 3A(iii). The Ino80-myc occupancies are additionally correlated with those for both Snf2-myc and Sth1-myc (S9A(ii)-(iii) Fig). Importantly, the median occupancies of Snf2-myc, Sth1-myc, and Ino80-myc for all 5' sites were significantly greater on induction of Gcn4 by SM compared to uninduced cells (Fig 3C(i)-(iii)). Together, these findings suggest that Gcn4 directly recruits SWI/SNF, Ino80C, and to a lesser degree RSC, to its 5' binding sites.

Supporting this last conclusion, we showed previously that Gcn4 directly interacts with SWI/SNF and RSC in cells extracts in a manner dependent on key hydrophobic residues in the Gcn4 activation domain crucial for activation of Gcn4 target genes [48,49]. Moreover, we showed that recruitment of both SWI/SNF and RSC to the *ARG1* UAS in SM-treated cells, as judged by ChIP analysis of Snf2-myc and Rsc8-myc, was diminished by deletion of *GCN4* [49]. Confirming our conclusion reached above that Gcn4 also recruits Ino80C, we found here that Ino80-myc occupancies at the 5' Gcn4 peaks were diminished by deletion of *GCN4*, particularly under inducing conditions (S9B(iii) & (iv) vs. (i)-(ii) Fig; S9C Fig, col. 3–4 vs. 1–2). Together with the above findings that Snf2-myc, Sth1-myc, and Ino80-myc occupancies peak in the vicinity of the Gcn4 binding motifs at the majority of 5' sites (Figs 3A and S8), that occupancies of all three CRs are induced in parallel with Gcn4 induction by SM (Fig 3C) and are positively correlated with Gcn4 occupancies for the group of 5' genes (Fig 3B), we consider it very likely that SWI/SNF, RSC, and Ino80C are all recruited directly by Gcn4 to the majority of 5' genes.

We next sought evidence that SWI/SNF acts directly to dissociate Gcn4 from the 5' binding sites where it negatively regulates Gcn4 binding. Sorting the 5' motifs according to their increases in Gcn4 occupancy in *snf2Δ\_I* versus WT\_I cells (Fig 3D (i)-(iii)), we found that Snf2-myc occupancies are generally higher at the 5' motifs exhibiting the largest increases in

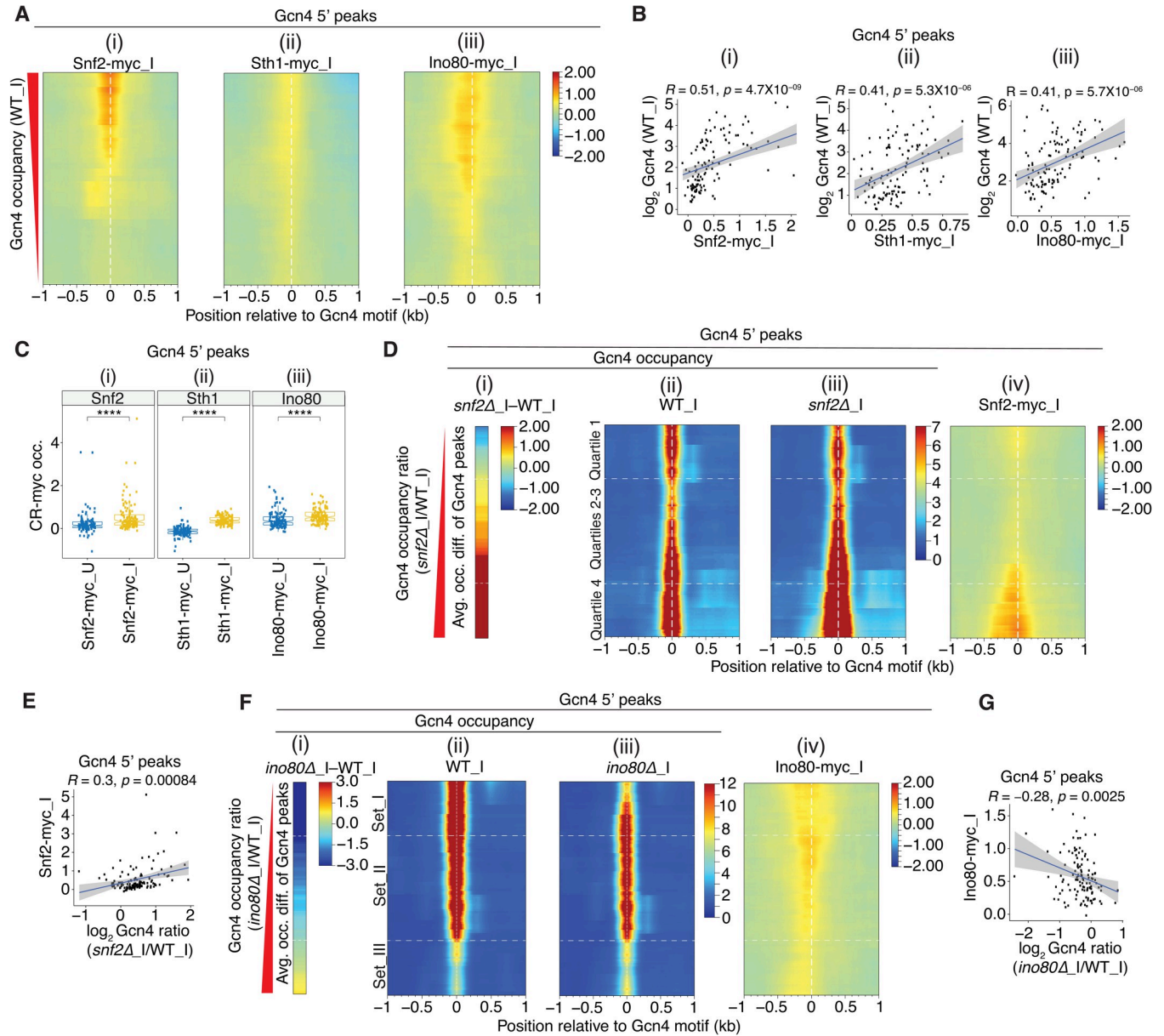


**Fig 3. All three CRs are recruited near the Gcn4 motifs at 5' sites.** (A) Heat map depictions of corrected SM-induced occupancies for (i) Snf2-myc, (ii) Sth1-myc and (iii) Ino80-myc (corrected by subtracting the background myc-occupancies from untagged WT\_I cells as described in Methods) at the 5' Gcn4 peaks, sorted by decreasing Gcn4 occupancies in WT\_I. Occupancies of the myc-tagged CR subunits were calculated from ChIP-seq data of mildly sonicated chromatin from 2 biological replicates for Snf2-myc\_I and Sth1-myc\_I, and 3 biological replicates for Ino80-myc\_I. (B) Scatterplots of log<sub>2</sub> Gcn4 occupancies in WT\_I vs. corrected occupancies for (i) Snf2-myc\_I, (ii) Sth1-myc\_I, or (iii) Ino80-myc\_I within ±100 bp windows surrounding the Gcn4 motifs of 5' sites. Pearson correlation coefficients (*R*) and associated *p* values are indicated. (C) Notched box plots of (i) Snf2-myc, (ii) Sth1-myc, or (iii) Ino80-myc corrected occupancies per nucleotide within ±100 bp windows surrounding the Gcn4 motifs of 5' sites in uninduced (\_U) and SM induced (\_I) conditions. (D) Heat maps depicting differences in Gcn4 occupancies between *snf2Δ*\_I and WT\_I cells (i); Gcn4 occupancies surrounding the motifs of 5' sites in (ii) WT\_I or (iii) *snf2Δ*\_I cells; and (iv) Snf2-myc\_I corrected occupancies surrounding the Gcn4 motifs of 5' sites. Gcn4 5' sites were sorted by increasing order of the ratio of Gcn4 occupancies in *snf2Δ*\_I vs. WT\_I cells. (E) Scatterplot of corrected Snf2-myc occupancies within ±100 bp windows surrounding the Gcn4 motifs of 5' sites vs. the log<sub>2</sub> ratios of Gcn4 occupancies in *snf2Δ*\_I vs. WT\_I cells at 5' Gcn4 peaks. Pearson correlation coefficients (*R*) and associated *p* values are indicated. (F) Heat maps depicting differences in Gcn4 occupancies between *ino80Δ*\_I and WT\_I cells (i); Gcn4 occupancies surrounding the motifs of 5' sites in (ii) WT\_I or (iii) *ino80Δ*\_I cells; and (iv) corrected Ino80-myc\_I occupancies surrounding the Gcn4 motifs of 5' sites. Gcn4 5' sites were sorted by increasing order of the ratio of Gcn4 occupancies in *ino80Δ*\_I vs. WT\_I cells, and the first (Set\_I, *n* = 30), middle two (Set\_II, *n* = 57) and fourth (Set\_III, *n* = 30) quartiles of fold-changes are depicted. (G) Same analysis shown in (E) except for corrected Ino80-myc occupancies vs. the log<sub>2</sub> ratios of Gcn4 occupancies in *ino80Δ*\_I vs. WT\_I cells.

<https://doi.org/10.1371/journal.pgen.1010277.g003>

Gcn4 occupancies conferred by the *snf2Δ* single mutation (and thus most negatively regulated by SWI/SNF), which are positioned at the bottom of the heat map in Fig 3D(iv); and that there is a significant positive correlation between these two parameters for all 5' sites (Fig 3E). Interestingly, a small enrichment of Snf2-myc is also evident for the 5' sites located at the top of the map in Fig 3D(iv), containing the subset of sites where SWI/SNF stimulates rather than impedes Gcn4 binding in WT cells. Overall, these findings support the idea that in WT cells containing RSC, SWI/SNF directly regulates Gcn4 binding at 5' sites, reducing binding at many sites but enhancing Gcn4 binding at a small subset of sites.

Carrying out the same analysis for Ino80C reveals that the 5' sites showing the strongest reductions in Gcn4 binding conferred by *ino80Δ* (at the top of the heat maps in Fig 3F(i)-(iii)) tend to have higher Ino80-myc occupancies (Fig 3F(iv)), in this case producing a negative correlation between the two parameters (Fig 3G). The correlation is likely weakened by the moderate enrichment for Ino80-myc at the bottom of the heat map for the 5' sites that show moderately increased Gcn4 binding in *ino80Δ* cells (Fig 3F(iv)). The elevated Ino80-myc occupancies at these latter sites could be explained by an inhibitory effect of Ino80C on Gcn4 binding, akin to our findings for SWI/SNF. Together, these results suggest that Ino80C also directly regulates Gcn4 binding at 5' sites, functioning like RSC to enhance binding at most sites but possibly mimicking SWI/SNF in reducing Gcn4 occupancy at a small subset of binding sites. Our findings that RSC and Ino80C are recruited to 5' sites on SM induction, and generally enhance Gcn4 occupancies, suggest that they function in a positive feedback loop. The fact that SWI/SNF is also highly recruited to 5' sites where it generally reduces Gcn4 occupancies (at least in WT cells), suggests that SWI/SNF acts directly to dampen the positive feedback loop established by the other CRs.

### Reduced Gcn4 occupancies are frequently associated with defective nucleosome eviction at Gcn4 binding motifs in mutants depleted of Sth1

The most likely mechanism for regulation of Gcn4 binding by CRs is the displacement of nucleosomes to either expose the motif and enhance binding or to occlude the motif and impede binding. ChIP-seq analysis of histone H3 in sonicated chromatin reveals reduced H3 occupancies surrounding the Gcn4 motifs within the NDRs of genes harboring 5' binding sites on SM induction of WT cells (Fig 4A, yellow vs. blue). These reductions in H3 seen in WT are diminished to similar extents in the *snf2Δ* and *P<sub>TET</sub>-STH1* single mutants, but to a greater extent in the *snf2Δ P<sub>TET</sub>-STH1* double mutant (Fig 4A, grey, red, & cyan vs. yellow), indicating cooperation between RSC and SWI/SNF in evicting nucleosomes at 5' Gcn4 sites. Similar conclusions were reached independently from H3 MNase ChIP-seq analysis of the same mutants (S10A Fig).

To examine the relationship between defects in H3 eviction and Gcn4 binding at particular 5' sites, we first plotted the changes in H3 occupancies in *snf2Δ P<sub>TET</sub>-STH1\_I* versus WT\_I cells in the regions surrounding the 5' Gcn4 motifs, sorted as above by their reductions in Gcn4 binding in this double mutant (Fig 4B(i)-(ii)). The resulting difference map reveals an obvious tendency for the 5' sites with the greatest reductions in Gcn4 binding, *ie.* in Sets\_1 and \_2 (dark blue hues in Fig 4B(i)), to exhibit sizable increases in H3 occupancies at the Gcn4 motifs in the double mutant (orange hues in Fig 4B(ii)), consistent with the idea that defective nucleosome eviction contributes to reduced Gcn4 binding in cells depleted of both RSC and SWI/SNF. Surprisingly, however, 5' sites at the bottom of the H3 difference map in Fig 4B(ii), belonging to Set\_3, also show marked increases in H3 occupancies, but exhibit the smallest changes in Gcn4 binding observed among all 5' sites in the double mutant (Fig 4B(i))—a complexity we address further below.

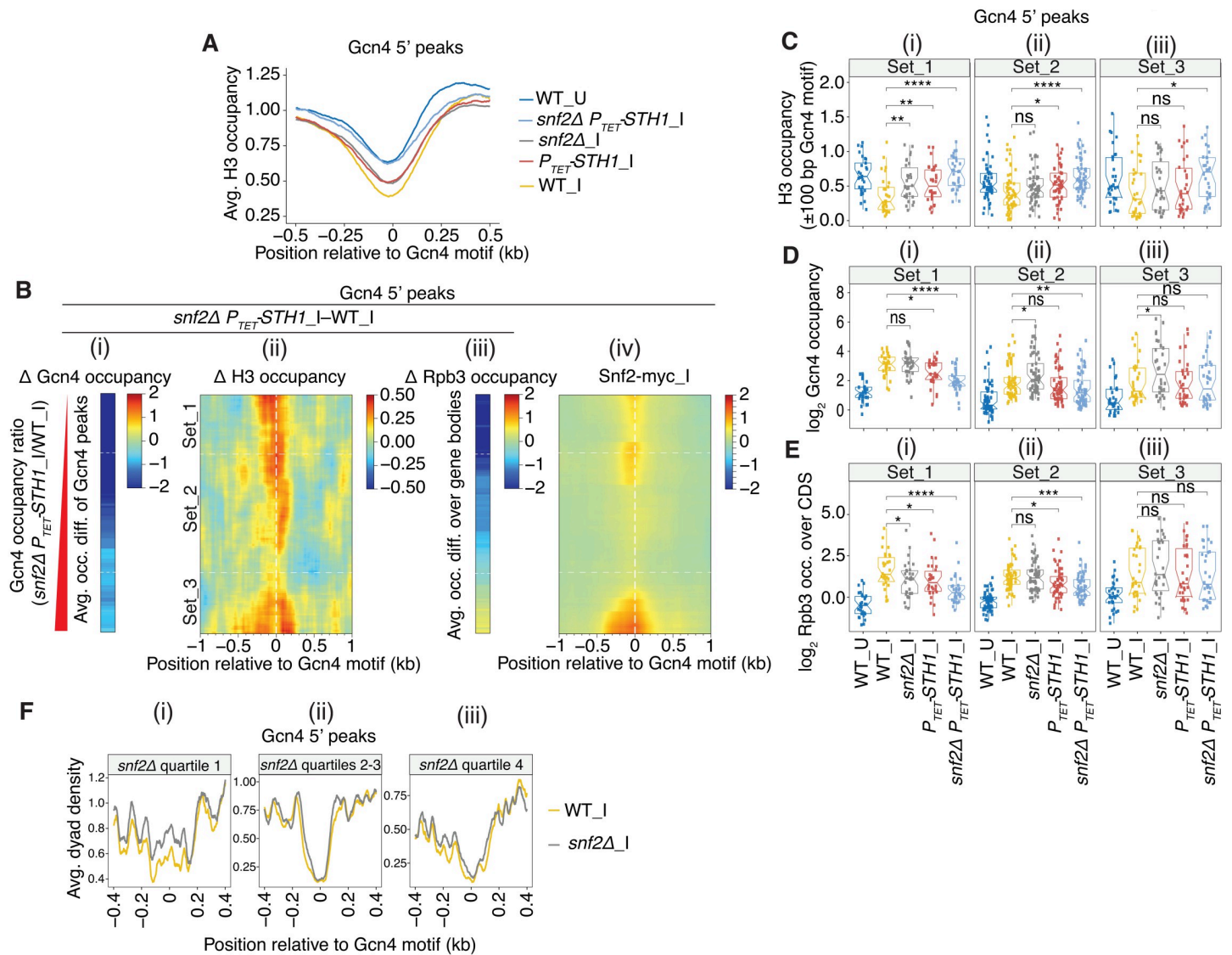


**Fig 4. Defective eviction of nucleosomes surrounding 5' Gcn4 motifs in SWI/SNF and RSC mutants.** (A) Plots of H3 occupancies at each base pair surrounding the Gcn4 motifs averaged over all 5' sites for the indicated strains/conditions, calculated from H3 ChIP-seq data. All of the average plots were found to converge at a position ~1.0 kb upstream and downstream of the Gcn4 motifs. (B) (i)-(iii) Heat maps depicting differences between *snf2Δ P<sub>TET</sub>-STH1\_I* and WT\_I cells for (i) Gcn4 occupancies measured as in Fig 2A(i), (ii) H3 occupancies surrounding the Gcn4 motifs of 5' sites from H3 ChIP-seq data, (iii) Rpb3 occupancies averaged over the CDS of 5' genes, for Gcn4 5' sites sorted by increasing order of fold-changes in Gcn4 occupancies in *snf2Δ P<sub>TET</sub>-STH1\_I* vs. WT\_I cells, as in Fig 2A and 2B. (iv) heat map of corrected Snf2-myc\_I occupancies surrounding the Gcn4 motifs for the same order of 5' sites as in (i)-(iii). (C-E) Notched box plots for the 3 sets of 5' sites defined in Fig 2A and 2B and indicated again in (B), depicting (C) H3 occupancies per base pair in the ±100 bp windows surrounding the Gcn4 motifs, (D) log<sub>2</sub> Gcn4 occupancies taken from Fig 2C, and (E) log<sub>2</sub> Rpb3 occupancies averaged over the CDS of genes with 5' sites. H3 and Rpb3 occupancies were calculated from ChIP-seq data of sonicated chromatin from at least 3 biological replicates of WT\_U, WT\_I, or *snf2Δ\_I*, *P<sub>TET</sub>-STH1\_I* and *snf2Δ P<sub>TET</sub>-STH1\_I* cells. (F) Average dyad densities calculated from H3 MNase-ChIP-seq data aligned to the Gcn4 consensus motifs, as described in Fig 1E, for the quartiles of 5' peaks defined in Fig 3D(i)-(ii) showing the smallest increases (and frequently decreases) in Gcn4 binding (i), intermediate increases (ii), or the largest increases in Gcn4 binding in *snf2Δ\_I* vs. WT cells (iii).

<https://doi.org/10.1371/journal.pgen.1010277.g004>

The aforementioned trends in the heat maps were examined more closely by quantifying the changes in H3 occupancies for a 200bp window surrounding the Gcn4 motifs and comparing them to the corresponding changes in Gcn4 occupancies in the different mutants. In WT cells, SM-induction confers the expected reduced median H3 occupancies in parallel with

increased Gcn4 occupancies for all three Sets of 5' sites (cf. Fig 4C and 4D, (i)-(iii), cols. 1–2). In both the  $P_{TET}\text{-}STH1$  and  $snf2\Delta P_{TET}\text{-}STH1$  mutants, the H3 occupancies are increased significantly for Set\_1 and Set\_2, and also for Set\_3 in the  $snf2\Delta P_{TET}\text{-}STH1$  double mutant, with larger increases in the double versus single mutant (Fig 4C(i)-(iii), cols. 4–5 vs. 2). Similar results were obtained by H3 MNase ChIP-seq analysis, except that no significant increase was observed for Set\_3 sites in either  $P_{TET}\text{-}STH1$  or  $snf2\Delta P_{TET}\text{-}STH1$  cells (S10B Fig). Importantly, the increased H3 occupancies at the Set\_1 sites are associated with decreased median Gcn4 occupancies in the  $P_{TET}\text{-}STH1$  and  $snf2\Delta P_{TET}\text{-}STH1$  cells, and the same applies to the Set\_2 sites in the double mutant (Fig 4D(i)-(ii), cols. 4–5 vs. 2). (The opposing changes in median H3 and Gcn4 occupancies shown in Fig 4C and 4D for Sets \_1 and \_2 are also evident for the corresponding biological replicates examined for WT and  $snf2\Delta P_{TET}\text{-}STH1$  cells, as shown in S1B and S1C Fig, cyan vs. yellow.) Similar insights emerged from a sectorized scatterplot of changes in H3 versus changes in Gcn4 occupancy in the double mutant compared to WT cells (S10C Fig), where nearly all of the 5' sites in Sets\_1 and \_2 (red and green points) fall into the upper left-hand quadrant exhibiting increased H3 but decreased Gcn4 occupancies in the double mutant. The association between reduced Gcn4 binding and increased H3 occupancies conferred by  $P_{TET}\text{-}STH1$  in the double mutant is also evident at the archetypal Set\_1 and Set\_2 genes depicted in S4A and S4B Fig. Together, these results support the conclusion that RSC and SWI/SNF (upon Sth1 depletion) cooperate in evicting nucleosomes to facilitate Gcn4 binding at most 5' sites belonging to Sets\_1 and \_2.

For the Set\_3 sites, by contrast, increased H3 occupancies are generally not associated with decreased Gcn4 binding in the  $snf2\Delta P_{TET}\text{-}STH1$  double mutant (cf. Fig 4C(iii) and 4D(iii), col. 5 vs. 2). As noted above, this conclusion applies even to the subset of sites at the bottom of the heat map in Fig 4B(ii) that show strong increases in H3 occupancies but exhibit the smallest reductions in Gcn4 binding among all 5' sites in response to the  $snf2\Delta P_{TET}\text{-}STH1$  double mutation. These latter sites exhibit high-level SWI/SNF recruitment (Fig 4B(iv), consistent with a direct role of SWI/SNF in nucleosome eviction, which has little impact on Gcn4 binding. The uncoupling of Gcn4 and H3 occupancies among Set\_3 sites is also evident in the scatterplot of S10C Fig, as these sites (blue points) show increases in H3 occupancies comparable to those found for Set\_1 and Set\_2 sites (red and green points) but much smaller decreases in Gcn4 binding. The uncoupling is particularly noteworthy for the Set\_3 archetype *ARG1* in the  $snf2\Delta P_{TET}\text{-}STH1$  double mutant (S4C(i) Fig). We concluded above that SWI/SNF exerts offsetting stimulatory and inhibitory effects on Gcn4 binding at the Set\_3 sites in the double mutant. Hence, to account for the uncoupling of changes in H3 and Gcn4 occupancies at Set\_3 sites, we suggest that elimination of SWI/SNF in the double mutant confers reduced nucleosome eviction at these sites, but the resulting increased H3 occupancies do not reduce Gcn4 binding owing to concurrent loss of a distinct function of SWI/SNF that inhibits Gcn4 binding.

Uncoupling of changes in H3 and Gcn4 occupancy is also widespread in the  $snf2\Delta$  single mutant. First, examining the sectorized scatterplot of H3 versus Gcn4 occupancy changes in S10D Fig shows that  $snf2\Delta$  increases the H3 occupancies for a large proportion of all 5' sites, with the majority of points mapping above the x-axis, but most points fall into the upper right-hand quadrant indicating increased Gcn4 binding conferred by  $snf2\Delta$ . Consistent with this, the  $snf2\Delta$  single mutation leads to increased median H3 occupancies at the Set\_1 sites (Fig 4C(i), col. 3 vs. 2), but has no effect on median Gcn4 binding at these sites (Fig 4D(i), col. 3 vs. 2). (See also S1B and S1C Fig for results from biological replicates for the Set\_1 sites in  $snf2\Delta_I$  vs. WT\_I cells, Set\_1, grey vs. yellow). The finding that increased H3 occupancies is generally not accompanied by decreased Gcn4 binding in  $snf2\Delta$  cells can be explained, as suggested above, if

the reduced nucleosome eviction conferred by *snf2Δ* is offset by loss of the proposed SWI/SNF function that impedes Gcn4 binding.

Exploring further the changes in Gcn4 binding and H3 occupancies conferred by the *snf2Δ* single mutation using the heat map analysis shown in [S11A Fig](#) revealed that a small subset of Set\_1 sites, located at the top of the map in panel (i), show decreased, rather than increased, Gcn4 binding in *snf2Δ* cells. Interestingly, these sites also exhibit the largest increases in H3 occupancies among all 5' sites conferred by *snf2Δ*, as shown in panel (ii). To evaluate more completely the minority fraction of 5' sites where SWI/SNF stimulates rather than impedes Gcn4 binding in WT cells, we sorted all of the 5' sites by their reductions in Gcn4 occupancies in *snf2Δ* versus WT cells, placing those sites at the top of the heat map (in Quantile 1) of [S11B\(i\) Fig](#). Again, we observed that these sites exhibit the largest increases in H3 occupancies at the Gcn4 motifs among all 5' sites ([S11B\(ii\) vs. \(i\) Fig](#)). Hence, at this small subset of 5' sites, SWI/SNF plays the conventional role observed for RSC of evicting nucleosomes to promote Gcn4 binding, replacing or outweighing the negative effect of SWI/SNF on Gcn4 binding occurring at most 5' sites in WT cells containing RSC.

As described fully in [S12 Fig](#), analysis of the *ino80Δ* mutant provides evidence that Ino80C enhances Gcn4 binding at a subset of 5' sites in Set\_I (as defined in [S6A\(ii\) Fig](#)) by evicting nucleosomes surrounding the relevant binding motifs, which is highly similar to our findings above for the *P<sub>TET</sub>-STH1* single mutant ([Fig 4C and 4D](#), Set\_1 genes). The association between reduced Gcn4 binding and increased H3 occupancies at the Gcn4 binding sites conferred by *ino80Δ* is illustrated for *YHR162W* and *HIS4* in [S12E Fig](#).

The results described above indicate that reduced Gcn4 binding conferred by the mutations that impair RSC or Ino80C can be attributed at least in part to increased H3 occupancies found at the binding motifs in these mutants, whereas the effects of *snf2Δ* are more complex owing to the opposing roles that SWI/SNF plays in (i) stimulating Gcn4 binding via nucleosome eviction, and (ii) impeding Gcn4 binding by an unknown mechanism. An intriguing possibility for the latter inhibitory function would involve sliding of the remaining, non-evicted nucleosomes over the Gcn4 binding motifs, in a manner demonstrated previously for yeast SWI/SNF and the Gal4 DNA binding domain in vitro [41]. However, because we do not observe reduced H3 occupancies in *snf2Δ* cells over the 5' sites that exhibit the largest increases in Gcn4 binding in this mutant ([S11B\(ii\) Fig](#), quartile 4), it would be necessary to stipulate that the proposed sliding is transitory and does not produce increased steady-state H3 occupancies over the 5' sites in WT versus *snf2Δ* cells. In this event, it might be expected that the nucleosome positions would be “fuzzier” in WT compared to the *snf2Δ* cells. Examining our H3 MNase ChIP-Seq data for *snf2Δ* and WT cells does not reveal a broader peak of nucleosome dyad positions encompassing the Gcn4 motifs for the Gcn4 sites with the largest increases in Gcn4 binding in *snf2Δ* cells ([Fig 4F\(iii\)](#), quartile 4 sites). A limitation of this last analysis is that there are very few nucleosomes that overlap the Gcn4 motifs at this group of sites, which are centered in the middle of NDRs, making it difficult to assess whether the nucleosome peaks exhibit the broadening expected for fuzzier positioning. However, there is also no obvious broadening of the adjoining -1 or +1 nucleosomes surrounding these sites ([Fig 4F\(iii\)](#)). In contrast, the 5' sites that exhibit decreased (versus increased) Gcn4 binding in *snf2Δ* cells exhibit increased nucleosome dyad densities at the binding motifs ([Fig 4F\(i\)](#), quartile 1 sites), consistent with the H3 ChIP-Seq data shown in [S11B\(ii\) Fig](#) for these sites (at the top of the map), and is to be expected if SWI/SNF stimulates Gcn4 binding by evicting nucleosomes at these motifs. In summary, we have no direct evidence that SWI/SNF impedes Gcn4 binding at certain 5' sites by sliding nucleosomes over the binding motifs; accordingly, the inhibitory effect could involve another biochemical activity of SWI/SNF, or it could arise as an indirect consequence of impaired nucleosome eviction at another genomic location.



## A combination of impaired Gcn4 binding and nucleosome eviction is associated with reduced transcription in the CR mutants

We asked next whether the reductions in Gcn4 binding at 5' sites in the  $P_{TET}$ - $STH1$  and  $snf2\Delta$   $P_{TET}$ - $STH1$  mutants confer reduced transcription of the associated genes. Indeed, for genes in Set\_1 and Set\_2, decreased Gcn4 binding is generally associated with reduced Rpb3 occupancies averaged over the downstream CDS in  $snf2\Delta$   $P_{TET}$ - $STH1$ \_I versus WT\_I cells. This trend is evident in both the heat-maps of Fig 4B (panel (iii) vs. (i), Sets\_1–2) and in box-plot comparisons of median occupancies of Rpb3 (Fig 4E(i)–(ii), col. 5 vs. 2) versus Gcn4 (Fig 4D(i)–(ii), col. 5 vs. 2) for the Set\_1 and Set\_2 genes. A similar association between reduced Rpb3 and diminished Gcn4 occupancies was found for the Set\_1 and Set\_2 genes in the  $P_{TET}$ - $STH1$  single mutant (Figs 4E(i)–(ii), col. 4 vs. 2) & S11C(iii) vs. (i) Fig). Note however that these genes also exhibit increased promoter H3 occupancies in the  $snf2\Delta$   $P_{TET}$ - $STH1$  and  $P_{TET}$ - $STH1$  mutants (Fig 4C(i)–(ii) (cols. 4–5 vs. 2), which might contribute to their reduced transcription owing to impaired PIC assembly.

The genes in Set\_3 exhibit increased promoter H3 levels in the  $snf2\Delta$   $P_{TET}$ - $STH1$  double mutant (Fig 4C(iii), col. 5 vs. 2), which appear to be insufficient to impair transcription (Fig 4E (iii), col. 5 vs. 2). Given the nearly WT Gcn4 occupancies of the Set\_3 genes in this mutant (Fig 4D(iii), col. 5 vs. 2), one possibility is that a reduction in Gcn4 binding is required in addition to defective nucleosome eviction for impaired transcription, as observed above for genes in Sets\_1 and 2 in the double mutant, perhaps owing to diminished recruitment of other coactivators by Gcn4 at its reduced occupancies. This inference can also account for the finding that the  $snf2\Delta$  single mutation reduces transcription of only the Set\_1 genes at the top of the difference heat maps in S11A(i)–(iii) Fig, which exhibit both reduced Gcn4 binding and marked increases in promoter H3 occupancies. Analysis of the  $ino80\Delta$  mutant by the same approaches, described fully in S12 Fig, likewise provides evidence that a combination of defects in Gcn4 binding and impaired promoter nucleosome eviction conferred by  $ino80\Delta$  reduces the transcription of a subset of genes with 5' Gcn4 binding sites.

## Evidence that the CRs stimulate TBP recruitment at SM-induced genes by evicting or displacing the +1 nucleosome

We examined next the contributions of SWI/SNF and RSC to PIC assembly at genes with 5' Gcn4 binding sites by conducting ChIP-seq of native TBP in the same CR mutants described above. The averaged occupancy plots revealed strong induction of TBP binding on SM treatment of WT cells, peaking ~130 bp downstream of the 5' motifs (Fig 5A(i), yellow vs. blue). Lower-level TBP binding also was induced ~200 bp upstream of the motifs, consistent with activation of bidirectional promoters by Gcn4. Essentially identical results were obtained in WT cells treated with Dox prior to SM treatment (Fig 5A(ii), black vs. blue), which served as the WT control for the  $P_{TET}$ - $STH1$ , and  $snf2\Delta$   $P_{TET}$ - $STH1$  mutants. The averaged TBP occupancies at both locations were substantially reduced in the SM-treated  $snf2\Delta$   $P_{TET}$ - $STH1$  double mutant and  $ino80\Delta$  strain (Fig 5A(ii), cyan vs. black; Fig 5A(i), gold vs. yellow), but were either unaffected or slightly increased, respectively, in the  $P_{TET}$ - $STH1$  and  $snf2\Delta$  single mutants (Fig 5A(ii), red vs. black; Fig 5A(i), grey vs. yellow). Interestingly, while not reducing TBP occupancies, the  $snf2\Delta$  mutation shifted the position of TBP binding upstream towards the Gcn4 binding site (Fig 5A(i) and 5C(ii)). The latter might indicate that TBP is recruited by Gcn4 to the UAS but is not efficiently delivered to the core promoter downstream, but additional work is required to understand the underlying mechanism. For Gcn4 motifs located within ORFs, induction of TBP occupancy peaks in WT cells was again observed both upstream and downstream of the motifs (S13A and S13B Fig), consistent with our

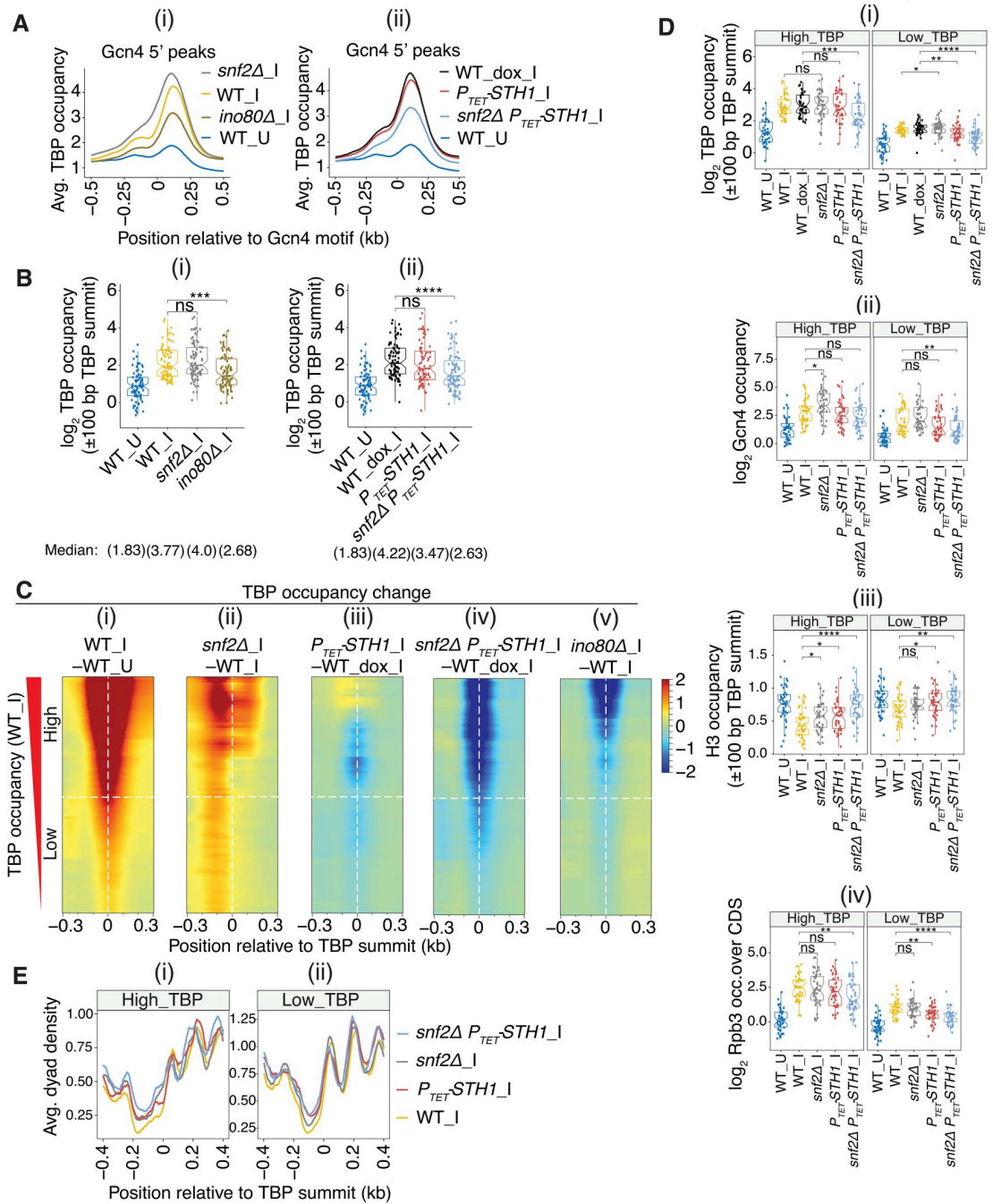


**Fig 5. Reduced TBP recruitment in SWI/SNF and RSC mutants is frequently associated with increased +1 nucleosome occupancies in promoters of genes with 5' Gcn4 binding sites.** (A) (i)-(ii) Averaged TBP occupancies surrounding Gcn4 5' motifs from ChIP-seq data of sonicated chromatin from at least 2 biological replicates of the indicated strains, with labels along the plots are arranged in decreasing order of summit heights. (B) (i)-(ii) Notched box plots of log<sub>2</sub> TBP occupancies measured within ±100 bp of TBP peak summits identified by MACS2 peak analysis in the promoters of 83 of the 5' Gcn4 target genes in the indicated yeast strains, color-coded as in (A). (C) Heat map depictions of differences in TBP occupancies surrounding TBP peak summits in the 83 5' genes from (B) sorted in decreasing order of *WT\_I* TBP levels in (i) *WT\_I* vs. *WT\_U*, (ii) *snf2Δ\_I* vs. *WT\_I*, (iii) *P<sub>TET</sub>-STH1\_I* vs. *WT\_I*, (iv) *snf2Δ P<sub>TET</sub>-STH1\_I* vs. *WT\_I*, and (v) *ino80Δ\_I* vs. *WT\_I*, color-coded as indicated to the right. Two equal bins based on *WT\_I* TBP of High\_TBP or Low\_TBP occupancies are indicated. (D) Notched box plots of factor occupancies in the 83 5' gene promoters for the two bins defined in (C) for (i) log<sub>2</sub> TBP within ±100 bp of TBP peak summits, (ii) log<sub>2</sub> Gcn4 at the respective Gcn4 peaks, (iii) H3 within ±100 bp of the TBP peak summits, and (iv) log<sub>2</sub> Rpb3 within the CDS of target genes. (E) Average dyad density from H3 MNase-ChIP-seq data aligned to the TBP summits of the 83 5' genes binned as in (C). Midpoints (dyads) of nucleosomal size sequences between 125 and 175 bp were averaged and plotted relative to the TBP

summits. Profiles were smoothed using a moving average filter with a span of 31 bp. Yeast strain labels are arranged in decreasing order of dyad densities at the +1 nucleosome spanning the TBP summits.

<https://doi.org/10.1371/journal.pgen.1010277.g005>

identification of bidirectional antisense and subgenic sense transcripts induced by internal Gcn4 binding [46]. As above, the averaged TBP occupancies within ORFs was markedly reduced only in the *snf2Δ P<sub>TET</sub>-STH1* double mutant and the *ino80Δ* strain (S13A and S13B Fig).

To quantify the effects of the CR mutations on TBP recruitment at individual genes with 5' Gcn4 peaks, we determined the TBP occupancies in a window of  $\pm 100$  bp surrounding the summits of each TBP peak that we identified at 83 of the 117 genes with 5' Gcn4 sites. Consistent with the averaged TBP data in Fig 5A, the results revealed significant reductions in median TBP occupancies only in the *snf2Δ P<sub>TET</sub>-STH1* and *ino80Δ* mutants compared to WT\_I cells (Fig 5B(i)-(ii)). We also displayed the TBP occupancy changes gene-by-gene using TBP difference heat maps in which the 5' genes were sorted by their TBP occupancies in WT\_I cells. As might be expected, the genes with highest TBP occupancies in WT\_I cells also display the largest inductions of TBP binding on SM-treatment of WT cells (Fig 5C(i), High vs. Low group). Most of the genes in the High\_TBP group (upper half of each map) show reductions in TBP binding in both the *snf2Δ P<sub>TET</sub>-STH1* and *ino80Δ* mutants compared to WT induced cells (Fig 5C(iv)-(v)); whereas only about one-half of these genes exhibit even moderately reduced TBP binding in the *P<sub>TET</sub>-STH1* single mutant (Fig 5C(iii)), and none show reduced TBP binding in *snf2Δ\_I* vs. WT\_I cells (Fig 5C(ii)). Together, the results in Fig 5A–5C indicate overlapping functions of RSC and SWI/SNF in promoting TBP recruitment on Gcn4 binding at 5' sites, wherein a strong recruitment defect occurs only when both Sth1 and Snf2 are removed simultaneously in the *snf2Δ P<sub>TET</sub>-STH1* double mutant. In contrast, eliminating Ino80 confers a marked reduction in TBP recruitment in otherwise WT cells at most of the genes exhibiting the highest levels of TBP recruitment by Gcn4 in WT cells.

Recently, we provided evidence that reductions in Pol II occupancies in *ino80Δ* cells are associated with both decreased TBP occupancies and increased promoter H3 occupancies at the SM-induced genes, consistent with the idea that Ino80C promotes Gcn4-activated PIC assembly and transcription by evicting promoter nucleosomes [26]. To extend this model to include RSC and SWI/SNF, we quantified the H3 occupancies surrounding the summits of the TBP peaks for the High\_TBP and Low\_TBP groups of 5' genes defined above. As expected, these H3 occupancies are reduced on SM-treatment of WT cells (Fig 5D(iii), High\_ & Low\_TBP, cols 1–2), consistent with eviction of promoter nucleosomes to facilitate TBP binding. Importantly, we observed increased H3 occupancies in the *snf2Δ P<sub>TET</sub>-STH1* double mutant that are greater in magnitude than observed in the *snf2Δ* or *P<sub>TET</sub>-STH1* single mutants under inducing conditions, particularly for the High\_TBP group (Fig 5D(iii), High\_ & Low\_TBP, cols 3–5 vs. 2). We also examined the positions of nucleosome dyads measured by H3 MNase ChIP-Seq analysis, which revealed a shift upstream in the averaged dyad densities of +1 nucleosomes that results in greater dyad densities immediately 5' of the TBP summits in the mutants, which was most pronounced in the double mutant for the High\_TBP group (Fig 5E(i)–5(ii), cyan vs. grey & red vs. yellow). The fact that combining the *snf2Δ* and *P<sub>TET</sub>-STH1* mutations in the double mutant confers additive increases in nucleosome occupancies at TBP binding sites that are coupled with additive reductions in TBP recruitment at many of these sites (noted above in Fig 5D(i), cols. 6 vs. 4–5) supports the model that RSC and SWI/SNF functionally cooperate to enhance Gcn4-activated TBP binding by eviction and repositioning of +1 nucleosomes. The coupling of reduced TBP binding and elevated H3 occupancies in the *snf2Δ P<sub>TET</sub>-STH1* double mutant is illustrated for six archetypal genes with 5' Gcn4 sites in

[S14A and S14B\(i\)-\(iii\) Fig.](#) The unexpected increase in TBP recruitment in the *snf2Δ* strain evident in [Fig 5C\(ii\)](#) might arise from the elevated Gcn4 binding found at most 5' sites in this mutant ([Fig 5D\(ii\)](#), cols. 3 vs. 2), which could increase recruitment of the cofactors serving as TBP adaptors, SAGA and TFIID, to elevate TBP recruitment despite somewhat higher +1 nucleosome occupancies.

Consistent with our previous findings [26], reduced TBP recruitment conferred by *ino80Δ* at genes with 5' Gcn4 sites also is frequently associated with elevated H3 occupancies at the TBP binding sites ([S13C \(i\)-\(ii\) Fig.](#)), as illustrated for four archetypal genes in [S13D and S13E Fig.](#)

Finally, as might be expected, the Pol II (Rpb3) occupancies in WT\_I cells are greater for the High\_TBP versus Low\_TBP group of genes containing 5' Gcn4 sites ([Fig 5D\(iv\)](#), High\_ vs. Low\_, col. 2). Importantly, we observed marked reductions in Rpb3 occupancies at these genes only in the *snf2Δ P<sub>TET</sub>-STH1* double mutant, with smaller reductions in the *P<sub>TET</sub>-STH1* single mutant and no significant changes in the *snf2Δ* single mutant ([Fig 5D\(iv\)](#), cols. 3–5 vs. 2). The fact that the changes in Pol II occupancies generally parallel the changes in TBP occupancies in these mutants (noted above in [Fig 5D\(i\)](#) and [Fig 5C\(ii\)-\(iv\)](#)) supports the model that RSC and SWI/SNF functionally cooperate to enhance Gcn4-activated transcription of these genes by stimulating PIC assembly.

### SWI/SNF functions with RSC and Ino80C in TBP recruitment only at highly expressed genes in non-stressed cells

Having found that SWI/SNF, RSC, and Ino80C all participate in TBP recruitment at genes with 5' Gcn4 binding sites in starved cells ([Fig 5A and 5B](#)), we next examined their relative importance for this step of PIC assembly at genes expressed at high levels in non-starved cells (ie. not treated with SM). In the absence of stress, ~50% of Pol II and the transcriptional machinery is devoted to transcription of ribosomal protein genes (RPGs) [50]. Accordingly, we examined the RPGs as a group and divided the remaining constitutively expressed genes into ten deciles according to their Rpb3 occupancies. Interestingly, all four of the CR mutations conferred significantly decreased TBP occupancies at the RPGs, with the greatest reductions in the *snf2Δ P<sub>TET</sub>-STH1* double mutant ([Fig 6A](#)), comparable marked reductions in the *P<sub>TET</sub>-STH1* and *ino80Δ* single mutants, and somewhat smaller reductions in the *snf2Δ* single mutant ([Fig 6A](#)). These findings indicate functional cooperation between RSC and SWI/SNF, and a substantial contribution from Ino80C, in TBP recruitment at the RPGs. All of the mutants also displayed reduced Rpb3 occupancies at the RPGs, but here *snf2Δ* conferred reductions comparable to those observed in the *snf2Δ P<sub>TET</sub>-STH1* double mutant and the *ino80Δ* mutant, with lesser reductions in the *P<sub>TET</sub>-STH1* single mutant ([Fig 6B](#)). These last results might indicate that SWI/SNF makes an additional contribution to transcription beyond TBP recruitment at these genes.

Examining changes in TBP occupancies at the remaining genes reveals reduced TBP recruitment for the ~40% most highly expressed genes in Deciles 1–4 in all four CR mutants, albeit of smaller magnitude compared to the RPGs ([Fig 6C](#)). By comparison to the RPGs, SWI/SNF makes a smaller contribution than RSC for the genes in Deciles 1–4, such that reductions in TBP occupancies are smaller in the *snf2Δ* versus *P<sub>TET</sub>-STH1* single mutant, and similar in magnitude between the *P<sub>TET</sub>-STH1* single mutant and *snf2Δ P<sub>TET</sub>-STH1* double mutant ([Fig 6C](#), cols. 1–3 for Deciles 1–4). The effect of *ino80Δ* is relatively greater in comparison to the other mutants for Deciles 1–4 compared to that observed for the RPGs, being comparable to the *snf2Δ P<sub>TET</sub>-STH1* double mutant in reducing TBP recruitment for the former genes ([Fig 6C](#), Deciles 1–4, cols. 3–4). For most of the remaining genes in Deciles 5–9, it appears that

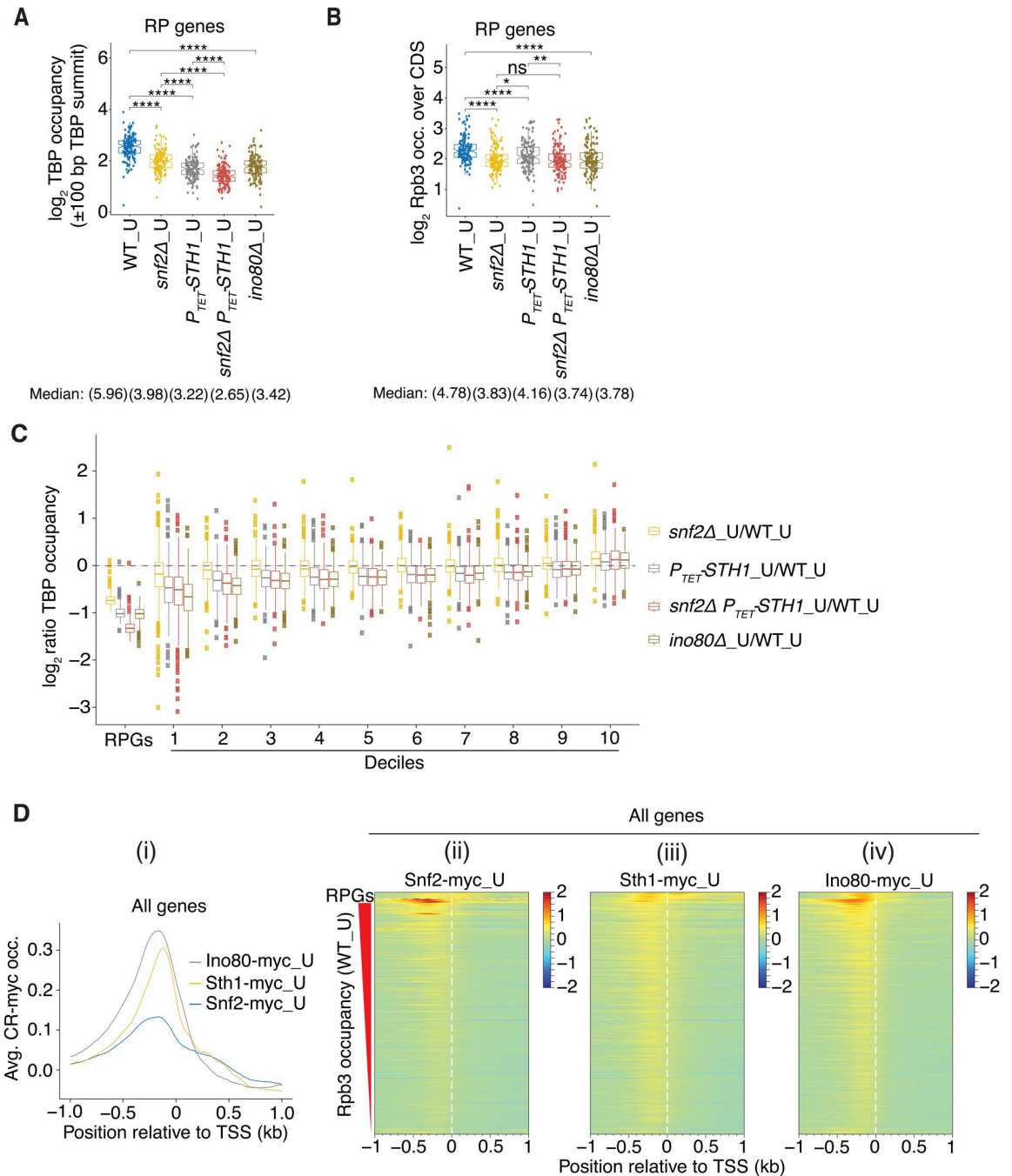


**Fig 6. RSC and Ino80C act broadly whereas SWI/SNF functions mainly at highly expressed genes to promote TBP recruitment.** (A-B) Notched box plots of  $\log_2$  TBP occupancies within  $\pm 100$  bp of TBP peak summits (A) and  $\log_2$  CDS Rpb3 occupancies (B) at all RP genes in WT or the indicated mutants, in uninduced cells. (C) Notched box plots of  $\log_2$  ratios of TBP occupancies in the indicated mutants vs. WT in uninduced cells for RP genes and Deciles 1–10 of all genes arranged in descending order of Rpb3 occupancies in WT\_U cells. (D) (i) Averaged corrected Ino80-myc\_U, Snf2-myc\_U, and Sth1-myc\_U occupancies aligned to the TSSs of all genes. (ii)–(iv) Heat map depictions of corrected occupancies of (ii) Snf2-myc\_U, (iii) Sth1-myc\_U, and Ino80-myc\_U (iv) at RP genes (at the top) and all other genes sorted in decreasing order of WT\_U Rpb3 levels, color-coded as indicated on the right.

<https://doi.org/10.1371/journal.pgen.1010277.g006>

RSC and Ino80C make comparable, modest contributions to TBP recruitment with little involvement of SWI/SNF, as we observe similar reductions in TBP occupancies in the  $P_{TET}$ - $STH1$ ,  $snf2\Delta$   $P_{TET}$ - $STH1$ , and  $ino80\Delta$  mutants, but no significant change in  $snf2\Delta$  cells (Fig 6C, Deciles 5–9, cols. 1–4). All of the mutants show somewhat elevated TBP occupancies for Decile 10 (Fig 6C, Decile 10, cols. 1–4), which might result from reduced competition with the more highly expressed genes whose ability to recruit TBP is impaired in the CR mutants. Overall, the results indicate that RSC and Ino80C function broadly to enhance TBP recruitment at constitutive genes regardless of gene expression levels, whereas SWI/SNF acts primarily at highly expressed genes, and particularly at the RPGs, to help stimulate this step of PIC assembly.

Examining averaged occupancies of Snf2-myc, Sth1-myc, and Ino80-myc at all genes in uninduced cells reveals enrichment of all three factors upstream of the TSS, with relatively higher averaged occupancies for Ino80-myc and Sth1-myc versus Snf2-myc (Fig 6D(i)). Interrogating individual genes using heat maps, sorting genes by Rpb3\_I occupancies, shows that Sth1-myc and Ino80-myc are moderately enriched upstream of the TSS at nearly all genes, whereas Snf2-myc is more restricted to highly expressed genes near the top of the map (Fig 6D(ii)-6(iv)). Thus, the relative occupancies of RSC, SWI/SNF, and Ino80C generally parallel their relative importance for TBP recruitment at these gene groups, which is consistent with direct contributions of the three CRs to this step of PIC assembly throughout the genome.

Finally, we compared the dependence on the three remodelers for TBP recruitment between genes that rely primarily on TFIID or utilize SAGA in addition to TFIID for this step of PIC assembly. The 655 genes designated as coactivator-redundant, which exhibit overlapping functions for SAGA or TFIID [51], show greater reductions in TBP in the  $P_{TET}$ - $STH1$ ,  $snf2\Delta$   $P_{TET}$ - $STH1$ , and  $ino80\Delta$  mutants than do the 4245 genes that rely primarily on TFIID (S15 Fig). Consistent with this, the most highly transcribed decile of the 4680 non-RPG genes (Decile 1), shown above to exhibit the greatest TBP reductions in all four remodeler mutants among all deciles (Fig 6C), are highly enriched for coactivator-redundant genes (53%) compared to Deciles 2–10 (5–19% coactivator-redundant genes) and the non-RPG genes as a group (~14%). Moreover, the genes with 5' Gcn4 sites, which show redundant contributions by SWI/SNF and RSC and a marked requirement for Ino80C for TBP recruitment (Fig 5B(i)-(ii)), are comprised of 45% coactivator-redundant genes. These findings suggest a tendency for coactivator-redundant genes to show a greater requirement than TFIID-dependent genes for RSC and Ino80C, and also for SWI/SNF among the most highly expressed members, for robust TBP recruitment. Interestingly, the RPGs are dramatic exceptions to this tendency, as they exhibit the strongest reductions in TBP recruitment in all four CR mutants of any gene group we analyzed but are almost exclusively (95%) TFIID-dependent genes. Thus, while showing minimal dependence on SAGA, the high-level transcription achieved by the RPGs involves the concerted functions of all three CRs for efficient TBP recruitment.

## Discussion

In this report, we have provided evidence for distinct contributions of three CRs in regulating the binding of transcriptional activator Gcn4 at its numerous target genes, and illuminated functions of these CRs in controlling TBP recruitment for PIC assembly and transcription, both at Gcn4 target genes and more generally throughout the genome. Gcn4 binds in the NDRs of most of its target genes (5' sites), but within the CDS at a subset of activated genes (ORF sites) where it stimulates bidirectional transcription of antisense and subgenic sense transcripts as well as activating the 5'-positioned promoters [46]. We found that depleting or eliminating the catalytic subunits of RSC (Sth1) or Ino80C (Ino80) reduces Gcn4 occupancies at both 5' and ORF binding sites; with differential contributions of these two CRs at different

5' sites. Surprisingly, SWI/SNF functions oppositely at 5' sites in WT cells, generally reducing their Gcn4 occupancies, while having little effect at the ORF sites. In cells depleted of Sth1, by contrast, SWI/SNF functionally substitutes for RSC in promoting Gcn4 binding at both 5' and ORF sites, as eliminating Snf2 exacerbates the effect of depleting Sth1 in reducing Gcn4 occupancies at the sites most affected by depleting Sth1 alone from otherwise WT cells. These opposing effects of SWI/SNF appear to cancel out at the subset of 5' sites where SWI/SNF most strongly impedes Gcn4 binding in WT cells, such that the double mutation *snf2Δ P<sub>TET</sub>-STH1* has little effect on their Gcn4 occupancies. Ino80C also stimulates Gcn4 binding at 5' sites that are highly dependent on RSC, but it stimulates binding at other 5' sites that are largely independent of RSC, and where SWI/SNF impedes rather than enhances Gcn4 binding. Thus, our results have uncovered distinct contributions of these three CRs to Gcn4 binding at different 5' sites.

The Gcn4 binding motifs of 5' sites tend to reside in the center of NDRs, while the ORF motifs are generally located in linkers connecting genic nucleosomes, suggesting that Gcn4 binding is impeded by inclusion of its recognition sequence within nucleosomes [46]. Consistent with this, our results suggest that RSC and Ino80C enhance Gcn4 binding by removing nucleosomes from the binding motifs in NDRs. Thus, the subset of 5' sites showing decreased Gcn4 occupancies in the *P<sub>TET</sub>-STH1* single mutant or in the *ino80Δ* strain also tend to exhibit defective H3 eviction at these 5' sites in those mutants (Figs 4C and 4D(i) & S12B and S12C (i)). We observed similar inverse relationships between effects of the *snf2Δ P<sub>TET</sub>-STH1* double mutation on H3 and Gcn4 occupancies for the subsets of 5' sites showing the largest reductions in Gcn4 occupancies in this double mutant (Sets\_1 and \_2). This correlation was not evident however for the 5' sites that are least impaired for Gcn4 binding in the double mutant (Set\_3), where increased H3 occupancies were not accompanied by appreciable reductions in Gcn4 binding (Fig 4C and 4D, (iii) vs. (i)-(ii)), which we attributed to eliminating an inhibitory effect of SWI/SNF on Gcn4 binding at these sites by the *snf2Δ* mutation in the double mutant. The dual opposing effects of SWI/SNF on Gcn4 binding can also account for the fact that the 5' sites in Sets\_1 and \_2 show increased H3 occupancies in the *snf2Δ* single mutant but generally no reduction in Gcn4 binding (Fig 4C and 4D(i)-(ii)); and also that the sites in Set\_3 exhibiting the least effect of *snf2Δ* on H3 eviction show increased Gcn4 binding in this mutant (Fig 4C and 4D(iii)). Thus, the effect of *snf2Δ* on Gcn4 binding at any given site appears to reflect the relative importance of SWI/SNF in evicting nucleosomes (to enhance binding) versus its opposing role in diminishing Gcn4 binding.

The negative effect of SWI/SNF on Gcn4 binding in WT cells is not unprecedented. In vitro studies indicate that SWI/SNF can displace the Gal4 DNA binding domain from its DNA binding site by sliding a nucleosome across the binding site [41]; and human SWI/SNF was found to displace glucocorticoid receptor from its binding sequence in a reconstituted nucleosome array, contributing to the transient nature of GR interactions with the promoter in chromatin [42]. We considered the intriguing possibility that SWI/SNF functions similarly by sliding nucleosomes that have not been evicted from the NDR across Gcn4 binding motifs to displace bound Gcn4, offsetting the stimulatory effects of nucleosome eviction at these binding sites exerted by other CRs, and that the outcome of these opposing effects differs at different 5' sites. However, we failed to observe higher occupancies of H3 or greater densities of nucleosome dyads in WT cells at the motifs of 5' sites where *snf2Δ* increases Gcn4 binding, nor could we detect greater fuzziness of such nucleosomes or the adjoining -1 and +1 nucleosomes in WT cells that might reflect transient nucleosome sliding back and forth across the motifs. It is possible therefore that deleting *SNF2* increases Gcn4 binding indirectly, eg. altering the expression or activity of an unknown factor that either reduces Gcn4 affinity or competes with Gcn4 for binding motifs. One finding disfavoring such an indirect mechanism, however, is that Snf2

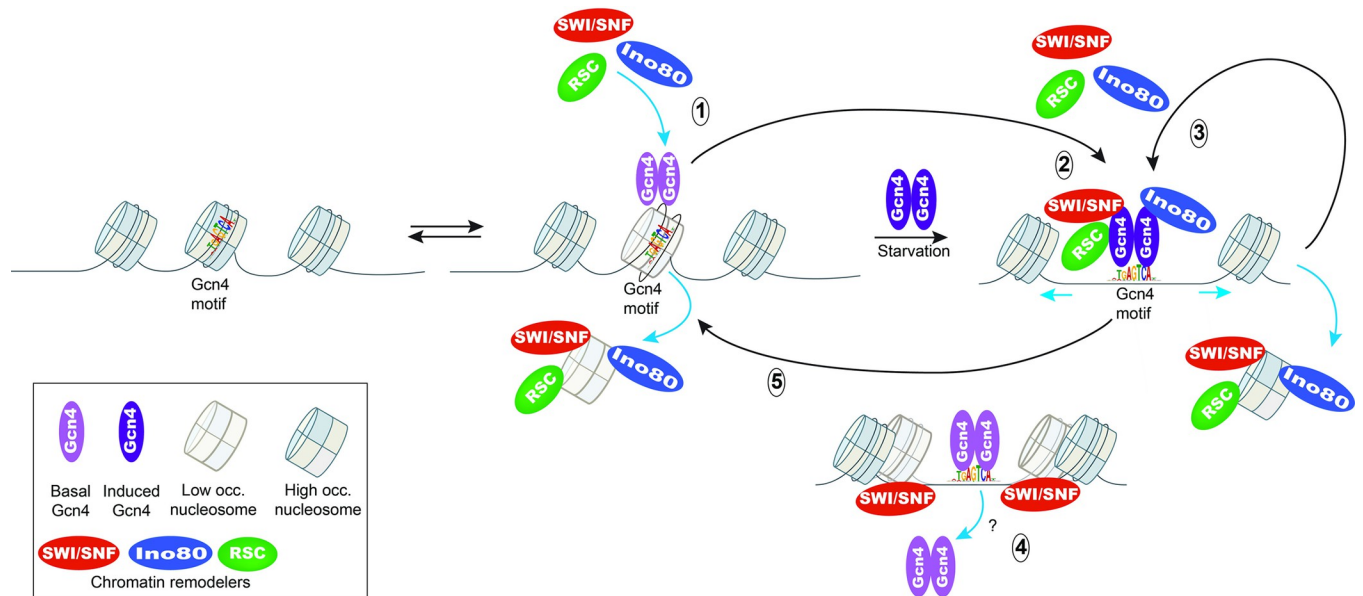


**Fig 7. Hypothetical model depicting a positive feedback loop involving SWI/SNF, RSC, and Ino80C in stimulating Gcn4 binding to motifs in NDRs of Gcn4 target genes.** (1) Basal recruitment of the three CRs reduces nucleosome occupancy of the Gcn4 binding motif in the NDR (depicted by a semi-transparent nucleosome) to facilitate binding of Gcn4 expressed at uninduced levels (light purple). (2) Induction of Gcn4 expression by amino acid starvation (dark purple) leads to increased Gcn4 binding by mass action. The increased Gcn4 occupancy leads to additional recruitment of the CRs, which in turn increases eviction and displacement of nucleosomes from the Gcn4 motif to favor additional Gcn4 binding, thus establishing a positive feedback loop that promotes Gcn4 binding (3). At a subset of binding sites, increased SWI/SNF recruitment enhances an inhibitory effect on Gcn4 binding by an unknown mechanism, leading to dissociation of Gcn4 from the NDR (4) and reversing the stimulatory effects of other CRs on Gcn4 binding (5).

<https://doi.org/10.1371/journal.pgen.1010277.g007>

occupancy at the Gcn4 sites is highly correlated with Snf2 function in suppressing Gcn4 binding (Fig 3D(i) vs. (iv)). Another possibility compatible with the latter is that SWI/SNF's direct interactions with Gcn4 itself [48,52] might dislodge Gcn4 from its binding motifs. Since the 5' motifs where SWI/SNF acts negatively are nearly devoid of nucleosomes, there would be no offsetting stimulatory effect of SWI/SNF through nucleosome eviction. Even in the case of RSC and Ino80C we cannot exclude the possibility that interactions of the CR with Gcn4 or other coactivators/PIC components influence Gcn4 binding independently of the established functions of the CRs in evicting or sliding nucleosomes.

By ChIP-seq analysis of myc-tagged versions of Sth1, Snf2, and Ino80, we obtained strong evidence that the CRs act directly to modulate Gcn4 binding at 5' sites, finding that their peak occupancies are centered around the Gcn4 binding motifs. These occupancies increased on induction of Gcn4 by SM treatment, consistent with widespread recruitment of the CRs by Gcn4 to UAS elements. Further evidence for the latter assertion was reported previously by demonstrating reduced SWI/SNF or RSC recruitment at the Gcn4 target gene *ARG1* in a *gcn4Δ* mutant [49,53], and similar evidence was obtained here for Gcn4-dependent Ino80-myc recruitment for the entire cohort of 5' Gcn4 binding sites. We envision that the basal levels of RSC and Ino80C stimulate Gcn4 binding to the UAS elements as Gcn4 abundance begins to rise in response to starvation, and that the bound Gcn4 then recruits higher levels of these two CRs to create a positive feedback loop of mutually stimulatory Gcn4 and CR binding/recruitment as induction proceeds (Fig 7). Even though it is not the most parsimonious explanation, we cannot rule out the alternative possibility that an unknown factor is responsible for recruiting Gcn4, RSC and Ino80C to higher levels in starved versus unstarved cells. Basal levels of SWI/SNF might similarly enhance Gcn4 binding during the early stages of induction, but the increasingly higher levels of SWI/SNF recruited as Gcn4 occupancy rises would frequently act



to impede Gcn4 binding in a manner that counteracts the enhanced Gcn4 binding stimulated by the other CRs. The basal levels of the CRs posited in this model could arise from stochastic interaction with NDRs, or from recruitment by basal levels of Gcn4 or other transcription factors bound to the UASs in non-starved cells. Presumably, the elevated occupancies of the CRs achieved at high-level Gcn4 binding enable them to diffuse laterally from the NDR to mediate the eviction and repositioning of the -1 and +1 nucleosomes we observed in starved WT cells [12,26,30].

Our model that Gcn4 stimulates its own binding by recruitment of CRs that evict nucleosomes from its binding sites (Fig 7) provides a molecular mechanism that may help to explain previous observations suggesting that an activation domain can facilitate DNA binding by the activator protein. Bunker and Kingston reported that tethering polycomb group proteins to a test promoter differentially interferes with promoter activation by various activation domains that were fused to the Gal4 DNA binding domain [54]. It is possible that the ability of an activation domain to recruit one or more CRs was instrumental in resisting the repressive effects of polycomb group proteins. Vashee and Kodadek found that the Gal4 activation domain could outperform the VP16 activation domain when each was linked to the Gal4 DNA binding domain for trans-activation specifically from weak Gal4 binding sites [55]. It is possible that the Gal4 AD was more efficient than the VP16 AD in recruiting CRs that eliminated nucleosomes surrounding the Gal4 binding sites in a manner that preferentially facilitated Gal4 binding to non-consensus motifs.

It seems likely that the increased nucleosome occupancies in the NDRs and core promoters of Gcn4 activated genes conferred by the CR mutations observed here and elsewhere [12,30] lead to reduced transcription initiation by occluding binding sites for TBP or other general transcription factors involved in PIC assembly. Indeed, we showed recently that reductions in Pol II occupancies in *ino80Δ* cells are associated with both decreased TBP occupancies and increased promoter H3 occupancies at the SM-induced genes [26]. Here, we observed additive reductions in TBP binding at genes with 5' Gcn4 sites on combining the *snf2Δ* and *P<sub>TET</sub>-STH1* mutations in the double mutant, which was associated with the additive effects of these mutations in elevating nucleosome occupancies at the TBP binding sites. The relatively smaller increases in H3 occupancies observed in the *P<sub>TET</sub>-STH1* or *snf2Δ* single mutants were associated with lesser reductions in TBP binding in the *P<sub>TET</sub>-STH1* cells than found in the double mutant, or even increased TBP binding in *snf2Δ* cells. The latter may reflect the elevated Gcn4 occupancies found at most 5' sites in *snf2Δ* cells, which might enable robust TBP recruitment despite increased nucleosome occlusion of the core promoters.

The functional cooperation between SWI/SNF and RSC in TBP recruitment observed at Gcn4 target genes in SM-treated cells was also observed in non-starved cells for the group of highly expressed RP genes, for which *snf2Δ* impaired TBP recruitment in otherwise WT cells and exacerbated the recruitment defect conferred by *P<sub>TET</sub>-STH1* in the double mutant. At the large majority of other genes, however, RSC is much more important than SWI/SNF in promoting TBP recruitment in non-starved cells, where it functions *on par* with Ino80C. The greater importance of RSC and Ino80C in TBP recruitment is mirrored by their greater occupancies compared to SWI/SNF at the majority of constitutively expressed genes. It is interesting that genes capable of utilizing SAGA or TFIID as a coactivator have a greater requirement for RSC and Ino80C compared to the genes that rely primarily on TFIID. Our findings support the idea that the three CRs act directly to enhance PIC assembly throughout the genome, with RSC and Ino80C acting broadly and with particular importance at coactivator-redundant genes, whereas SWI/SNF function is concentrated at certain highly expressed genes, including RP genes in non-starved cells and Gcn4-induced genes in amino acid-starved cells.

## Materials and methods

### Plasmid and yeast strain constructions

Yeast strains employed in this study are listed in [S1 Table](#). Yeast strains BY4741 (F729), F731 (*gcn4Δ*) and F748 (*snf2Δ*) were purchased from Research Genetics and described previously [56,57]. Constructions of *P<sub>TET</sub>-STH1* strain HQY1632 and *snf2Δ P<sub>TET</sub>-STH1* strain HQY1660 [12] and *ino80Δ* strain YR092 [26] were described previously; as were *SNF2-myc* (HQY367), *STH1-myc* (HQY459) [49] and *INO80-myc* (HQY1687) strains [26]. Strain HQY1718 (*gcn4Δ INO80-myc*) was constructed from F731 by a PCR-based method for tagging chromosomal genes by yeast transformation [58], using pFA6a-13Myc-His3MX6 DNA as PCR template. To deplete Sth1 from *P<sub>TET</sub>-STH1* strains, cells were cultured with 10 μg/μl doxycycline for 8–9h, and Sth1 depletion was confirmed by Western analysis.

### ChIP-seq and PCR ChIP analysis of Gcn4 occupancy

WT strain BY4741 and *snf2Δ* or *ino80Δ* mutant strains were cultured for at least 3 doublings in synthetic complete medium lacking isoleucine and valine (SC-Ilv) to log-phase ( $OD_{600} = 0.6–0.8$ ) and SM was added at 1 μg/ml for 25 min to induce Gcn4 synthesis. To transcriptionally deplete Sth1 from *P<sub>TET</sub>-STH1* and *snf2Δ P<sub>TET</sub>-STH1* strains, cells were cultured in SC-Ilv medium with 10 μg/μl doxycycline for 8–9h to log-phase ( $OD_{600} = 0.4–0.6$ ), allowing 2–3 doublings, and SM was added at 1 μg/ml for 25 min as above. ChIP-seq was conducted and DNA libraries for Illumina paired-end sequencing were prepared as described previously [12] except that chromatin samples containing 5 μg DNA were immunoprecipitated using Gcn4 antibodies [59] for 3h in experiments comparing WT with *snf2Δ* and *P<sub>TET</sub>-STH1* mutants, and overnight in experiments comparing WT and *ino80Δ* strains. Biological replicates of Gcn4 ChIP-seq data (and all other ChIP-seq data) are described in [S2 Table](#).

PCR-based ChIP analysis of Gcn4 occupancy at four target genes was performed as previously described [30].

### ChIP-seq analysis of TBP

For analyzing TBP occupancies, strains were cultured in the presence or absence of SM treatment and subjected to ChIP-seq analysis using antibodies against native TBP, as previously described [26].

### ChIP-seq analysis of *Snf2-myc<sub>13</sub>*, *Sth1-myc<sub>13</sub>* and *Ino80-myc<sub>13</sub>*

*SNF2-myc* and *STH1-myc* strains were cultured in the presence or absence of SM treatment, and untagged WT strain BY4741 cultured with SM, were subjected to ChIP-seq analysis as described previously [30] with a few modifications. Yeast cells (100 ml) were cross-linked for 15 min with 10 ml formaldehyde solution (50 mM HEPES KOH, pH 7.5, 1 mM EDTA, 100 mM NaCl and 11% formaldehyde) and quenched with 15 ml of 2.5 M glycine. WCEs were prepared by glass-beads lysis in 400 μl FA lysis buffer (50 mM HEPES KOH, pH 7.5, 1 mM EDTA, 150 mM NaCl, 1% TritonX-100 and 0.1% Na-deoxycholate) with protease inhibitors for 45 min at 4°C and the supernatant collected after removing the beads was pooled with 600 ml FA lysis buffer used for washing the beads. The resulting lysate was sonicated to yield DNA fragments of 300–500 bp and cleared by centrifugation. Chromatin samples containing 5.0 μg DNA were immunoprecipitated with anti-myc antibodies (Roche) for 3h. Paired-end sequencing libraries were prepared from immunoprecipitated DNA using Illumina paired-end kits from New England Biolabs (cat. #E7370 and #E7335). ChIP-seq analysis of *Ino80-myc* was previously described [26]. The myc occupancies at each nucleotide, normalized to the average

myc occupancy per nucleotide on the chromosome, were calculated for each myc-tagged strain and for the untagged WT and *gcn4Δ* strains, and the latter values were subtracted from the former values to yield the corrected occupancies of the myc-tagged CR subunits in the tagged strains.

### ChIP-seq analysis of Rpb3 and histone H3

ChIP-seq analysis of histone H3 (Abcam, Ab 1791) and Rpb3 (Neo-Clone, W0012) using formaldehyde cross-linked chromatin sheared by sonication were conducted as described previously [12,26,30]. Similarly, ChIP-seq analysis of histone H3 (Abcam, Ab1791) following micrococcal nuclease (MNase) digestion was carried out as described previously [12].

### Bioinformatics analysis of ChIP-seq data

Paired-end sequencing (50 nt from each end) was conducted by the DNA Sequencing and Genomics core facility of the NHLBI, NIH. Sequence data were aligned to the SacCer3 version of the genome sequence using Bowtie2 [60] with parameters *-X 1000—very-sensitive*, to map sequences up to 1 kb with maximum accuracy. PCR duplicates from ChIP-seq data were removed using the *samtools rmdup* package. Numbers of aligned paired reads from each ChIP-seq experiment and correlation coefficients for genome-wide occupancy profiles of the different replicates are summarized in S2 Table. Raw genome-wide occupancy profiles were obtained from the alignment (.bam) files by counting the number of DNA fragments that overlapped with every bp, using the *coverage* methods for *GRanges* objects from the GenomicRanges package in R. To allow the comparison between different samples, each profile was normalized such that the average occupancy for each chromosome was equal to one. Heat maps showing alignments of multiple loci were generated in R using custom scripts (<https://github.com/rchereji/bamR>). To visualize specific loci, *igvtools* was used to create tracks (*tdf* files) that were loaded in the Integrative Genomics Viewer (IGV, Broad Institute) [61]. Transcript end coordinates (TSS and TTS) were obtained from [62].

For calculation of per base pair occupancies in the given intervals, generation of averaged occupancies profiles and heat maps of occupancies or occupancy differences surrounding the given genomic features, a custom R scripts package available at [github.com/rchereji/bamR](https://github.com/rchereji/bamR) was employed. These R scripts, originally designed to plot ChIP-seq occupancies surrounding genic features like TSS and TTS or within coding sequences, were adapted to generate heat maps of Gcn4 occupancy differences within peak coordinates, TBP occupancy differences surrounding the peak summits, and histone H3 occupancies and nucleosome dyad densities surrounding Gcn4 motifs or TBP summits. To do so, alternative genome annotation files were generated with either Gcn4 peak start and end coordinates or 200 bp intervals surrounding the TBP peak summits replacing ORF start and end coordinates; and with Gcn4 motif centers or TBP peak summits replacing TSS coordinates. The annotation information employed for these analyses are provided in S1 File. Box plots, scatter plots and line plots were generated using R package “ggpubr”.

### Identification of TBP peaks

To identify TBP peaks in the gene promoters of Gcn4 5' target genes, MACS2 (<http://liulab.dfci.harvard.edu/MACS/>) analysis was employed to TBP ChIP-seq data from two replicates of WT\_I cultures (S2 Table), using a threshold for the p-value of  $10^{-3}$  (S1 File, sheet “MACS2\_TBP\_Ind”). Among 117 5' target genes, we identified TBP peaks in the promoters of 83 5' target genes (S1 File, sheet “TBP\_peak\_annotations”). MACS2 analysis of WT\_U TBP ChIP-seq data was conducted as above using a p-value of  $10^{-3}$  for identifying the TBP peak

within the promoter of 134 RP genes (S1 File, sheet “MACS2\_TBP\_Unind”). TBP peaks were assigned to specific genes by using the bedtools utility “closest” to identify the TBP peak summit closest to the TSS of each gene, followed by assessment of the TBP summit by examining the TBP data in the IGV browser. As tDNA genes often reside in the 5' non-coding regions of Pol II-transcribed genes and display large TBP peaks in both induced and uninduced conditions, the TBP occupancies within 250 bp surrounding tDNA genes (S1 File, sheet “tDNA\_annotations”) were subtracted from the TBP coverage in the bed file of merged replicate data and the corrected bed file was used to generate averaged profiles and calculate TBP occupancies within 200 bp intervals surrounding the TBP summits. The computation of TBP occupancies in the intervals comprised of 100 bp on either side of the TBP summits, as done in Fig 5B, was found to be unaffected if the TBP occupancies at neighboring tDNA genes were not subtracted in the manner just described.

## Data and software availability

File S1 contains (i) annotations of Gcn4 and TBP occupancy peaks listing the coordinates of the Gcn4 occupancy peaks or the windows of  $\pm 100$  bp surrounding the summits of each TBP peak used in plotting heat maps of Gcn4 or TBP occupancies, and (ii) results of MACS2 analysis of uninduced and SM induced TBP ChIP-seq data. A file listing the genomic coordinates of the 250 bp surrounding each tDNA gene is also provided in File S1. File S2 contains the data used to construct all plots. Unprocessed and analyzed ChIP-seq data have been deposited in the NCBI GEO database under accession number GSE192592

## Supporting information

**S1 Table. Yeast strains used in this study.** Names, genotypes and sources of each strain are given.

(DOCX)

**S2 Table. Compilation of ChIP-seq replicate experiments.** The strain and growth condition (SM-induced (I), or uninduced (U)), immunoprecipitating antiserum (IP), sample identification number, total number of sequencing reads (All PE reads), number of reads after removing duplicate reads (PE rmdup), correlation coefficient between indicated replicates, and source of data, are given for each ChIP-seq experiment.

(DOCX)

**S3 Table. PCR ChIP data for Gcn4 binding at four exemplar target genes.** Mean occupancies ( $\pm$  SEM or  $\pm$  SD) of Gcn4 in the UAS regions of the indicated genes is expressed as the ratio of input DNA recovered in the immunoprecipitates corrected for the same ratio measured for non-transcribed sequences from chromosome V (analyzed as a control for non-specific immunoprecipitation) as described previously [30].

(DOCX)

**S1 Fig. Supporting evidence that SWI/SNF and RSC have differential effects on Gcn4 binding at 5' sites. (A-B)** Box plots of  $\log_2$  Gcn4 occupancies in biological replicates of WT\_U, WT\_I, or *snf2 $\Delta$ \_I*, *P<sub>TET</sub>-STH1\_I* and *snf2 $\Delta$  P<sub>TET</sub>-STH1\_I* cells for all 5' sites (A), or in the three sets of Gcn4 5' sites defined in Fig 2B (B). (C) Box plots of H3 occupancies in biological replicates of WT\_U, WT\_I, or *snf2 $\Delta$ \_I*, *P<sub>TET</sub>-STH1\_I* and *snf2 $\Delta$  P<sub>TET</sub>-STH1\_I* cells for the three sets of 5' Gcn4 sites defined in Fig 2B.

(DOCX)

**S2 Fig. Supporting evidence that SWI/SNF and RSC have differential effects on Gcn4 binding at particular 5' sites.** Gene browser profiles of Gcn4 occupancies from biological replicates for the indicated strains/conditions. The Gcn4 peak numbering assigned previously [46] is given at the top of each profile, and the Gcn4 occupancies per nucleotide averaged over the peaks determined in this study are listed next to each peak. (DOCX)

**S3 Fig. Supporting evidence that SWI/SNF and RSC have differential effects on Gcn4 binding at 5' sites. (A-C)** Paired box plots of  $\log_2$  Gcn4 occupancies comparing (A) WT\_I versus  $P_{TET-STH1\_I}$ , (B)  $P_{TET-STH1\_I}$  versus WT\_I and  $snf2\Delta P_{TET-STH1\_I}$  and (C) WT\_I versus  $snf2\Delta I$  in 3 sets of Gcn4 5' sites comprised of the (i) first (Set\_1, n = 30), (ii) middle two (Set\_2, n = 57) and (iii) last (Set\_3, n = 30) quartiles of the fold-changes in Gcn4 occupancy in  $snf2\Delta P_{TET-STH1\_I}$  vs. WT\_I cells as depicted in Fig 2B(i). Lines connecting each data point in respective strains indicate changes in the Gcn4 occupancies of respective Gcn4 site. (D) Sectored scatterplot of the  $\log_2$  ratios of Gcn4 occupancies per base pair over the peak coordinates assigned by MACS2 analysis in  $snf2\Delta I$  vs. WT\_I cells versus the corresponding  $\log_2$  ratios of Gcn4 occupancies in  $snf2\Delta P_{TET-STH1\_I}$  vs. WT\_I cells. The 3 sets of Gcn4 5' sites defined in Fig 2B(ii) are color-coded as: Set\_1, red rectangles; Set\_2, green pluses; and Set\_3, blue stars. (DOCX)

**S4 Fig. Gene browser profiles of Gcn4 and H3 occupancies from ChIP-seq analyses of sonicated chromatin for representative genes in the indicated strains.** The Gcn4 peak numbering assigned previously [46] is given at the top of each profile, and the Gcn4 occupancies per nucleotide averaged over the peaks determined in this study are listed next to each peak. (DOCX)

**S5 Fig. Differential requirements for Ino80C and RSC for Gcn4 binding at a subset of Gcn4 5' sites. (A)** Heat maps of differences in Gcn4 occupancies averaged across the coordinates of 5' sites between the indicated mutant and WT\_I samples for (i)  $ino80\Delta I$  and (ii)  $snf2\Delta P_{TET-STH1\_I}$ . Gcn4 5' sites were sorted by increasing order of the ratio of Gcn4 occupancies in the double mutant  $snf2\Delta P_{TET-STH1\_I}$  vs. WT\_I. (B) Heat map depictions of Gcn4 occupancies surrounding the Gcn4 motifs of 5' sites in (i) WT\_I (for the  $ino80\Delta$  mutant), (ii)  $ino80\Delta I$ , (iii) WT\_I (for the  $snf2\Delta P_{TET-STH1\_I}$  mutant), and (iv)  $snf2\Delta P_{TET-STH1\_I}$  cells, for the same ordering of 5' sites as in (A). The sets of Gcn4 5' sites (Set\_1, Set\_2, and Set\_3) defined in Fig 2A and 2B are depicted in B(i). (C & D) Same analyses for  $ino80\Delta I$  and  $P_{TET-STH1\_I}$  as shown in (A-B) except for Gcn4 ORF sites. (DOCX)

**S6 Fig. Identification of Gcn4 5' sites with heightened Ino80C dependence for Gcn4 occupancy. (A)** Heat map depicting differences in Gcn4 occupancies between  $ino80\Delta I$  and WT\_I cells (i); Gcn4 occupancies surrounding the motifs of 5' sites in (ii) WT\_I or (iii)  $ino80\Delta I$  cells. Gcn4 5' sites were sorted by increasing order of the ratio of Gcn4 occupancies in  $ino80\Delta I$  vs. WT\_I cells, and the first (Set\_I, n = 30), middle two (Set\_II, n = 57) and fourth (Set\_III, n = 30) quartiles of fold-changes are depicted in A(ii). (B) Heat map depictions of differences in Gcn4 occupancies between (i)  $snf2\Delta P_{TET-STH1\_I}$  and WT\_I, (ii)  $P_{TET-STH1\_I}$  and WT\_I, and (iii)  $snf2\_I$  vs. WT\_I cells in same order as in S6A Fig. (C) Notched box plots of  $\log_2$  Gcn4 occupancy in WT\_U, WT\_I, and  $ino80\Delta I$  cells in 3 sets of Gcn4 5' sites comprised of the (i) first (Set\_I, n = 30), (ii) middle two (Set\_II, n = 57) and (iii) last (Set\_III, n = 30) quartiles of the fold-changes in Gcn4 occupancy in  $ino80\Delta I$  vs. WT\_I cells as defined in panel A(ii). P values for the significance of differences in medians calculated by the Mann-Whitney-Wilcoxon test are indicated. (D) Scatterplots of  $\log_2$  ratios of Gcn4 occupancy changes in WT\_I vs.  $ino80\Delta I$

cells plotted against  $\log_2$  Gcn4 occupancies in WT\_I cells for 5' (i) and ORF (ii) Gcn4 sites. Pearson correlation coefficients ( $R$ ) and associated  $p$  values are indicated.

(DOCX)

**S7 Fig. Supporting evidence that reduced Gcn4 binding in mutants depleted of RSC or Ino80C occurs preferentially at motifs of highest affinity or accessibility in chromatin in WT\_I cells.** (A & B) Histograms depicting (A)  $\log_2$  Rpb3 occupancies in the *GCN4* CDS measured by Rpb3 ChIP-seq, indicating transcription levels; and (B) Gcn4 protein levels measured previously [12] by Western blot analysis in the indicated strains using Gcd6 signals analyzed in parallel as loading control. Band intensities for Gcn4 were normalized to those for Gcd6 in the same samples and the mean Gcn4/Gcd6 ratios determined from 3 biological replicates were plotted. Significance of differences in mean values was calculated with the student's  $t$  test. (C & D) Scatterplots of  $\log_2$  WT\_I Gcn4 occupancies vs. motif FIMO scores [46] for (C) the 117 Gcn4 5' sites and (D) the 62 Gcn4 ORF peaks, using the motif of highest score for peaks with multiple motifs. Pearson correlation coefficients ( $R$ ) and associated  $p$  values are indicated. (E) Notched box plots of motif FIMO scores for the sets of Gcn4 5' sites binned according to the fold-changes in occupancy in *snf2Δ P<sub>TET</sub>-STH1\_I* vs. WT\_I cells, as depicted in Fig 2B.

(DOCX)

**S8 Fig. Gene browser profiles of Gcn4 and corrected Snf2-myc occupancies from ChIP-seq analyses of sonicated chromatin for the indicated strains.** The Gcn4 peak numbering assigned previously [46] is given at the top of each profile, and corrected Snf2-myc occupancies per nucleotide within  $\pm 100$  bp windows surrounding the Gcn4 motifs are listed next to each peak.

(DOCX)

**S9 Fig. Supporting evidence for recruitment of the three CRs by Gcn4 to its 5' sites.** (A) (i)-(iii) Scatterplots of corrected occupancies of the indicated myc-tagged CR subunits in WT\_I cells measured within  $\pm 100$  bp windows surrounding the Gcn4 motifs of 5' Gcn4 peaks. Pearson correlation coefficients ( $R$ ) and associated  $p$  values are indicated. (B) Heat map depictions of corrected Ino80-myc occupancies at the 5' Gcn4 peaks, sorted by decreasing Gcn4 occupancies in WT\_I cells and plotted relative to the Gcn4 motifs, for (i) uninduced *gcn4Δ* cells, (ii) SM-treated *gcn4Δ* cells, (iii) uninduced WT cells, and (iv) SM-treated WT cells. Occupancies were calculated from ChIP-seq data of mildly sonicated chromatin from 2 or 3 biological replicates each of isogenic *GCN4* or *gcn4Δ* strains, harboring *INO80-myc* or untagged *INO80*, under inducing or uninducing conditions, correcting the occupancies for *INO80-myc* cells for those measured for the untagged *INO80* cells of the same *GCN4* genotype and growth conditions. (C) Notched box plots of corrected Ino80-myc occupancies per nucleotide within  $\pm 100$  bp windows surrounding the Gcn4 motifs of 5' sites in uninduced (\_U) or SM induced (\_I) *gcn4Δ* or WT cells.

(DOCX)

**S10 Fig. Supporting evidence for defective eviction of nucleosomes surrounding 5' Gcn4 motifs in SWI/SNF and RSC mutants.** (A) Plots of H3 occupancies calculated from H3 MNase-ChIP-seq data at each base pair surrounding the Gcn4 motifs averaged over all 5' sites for the indicated strains/conditions. (B) Notched box plots for the 3 sets of 5' sites defined in Fig 2A and 2B depicting H3 occupancies per base pair in the  $\pm 100$  bp windows surrounding the Gcn4 motifs. H3 occupancies were calculated from H3 MNase-ChIP-seq data from at least 3 biological replicates of WT\_U, WT\_I, or *snf2Δ\_I*, *P<sub>TET</sub>-STH1\_I* and *snf2Δ P<sub>TET</sub>-STH1\_I* cells. (C-D) Sectorized scatterplots of the  $\log_2$  ratios of Gcn4 occupancies vs  $\log_2$  ratios of H3 occupancies per base pair in the  $\pm 100$  bp windows surrounding the Gcn4 motifs in *snf2Δ*

*P<sub>TET</sub>-STH1\_I* vs. WT\_I cells (C) or *snf2Δ\_I* vs. WT\_I cells (D). The 3 sets of Gcn4 5' sites defined in Fig 2B(ii) are color-coded as: Set\_1, red rectangles; Set\_2, green pluses; and Set\_3, blue stars.

(DOCX)

**S11 Fig. Defective eviction of nucleosomes associated with reduced Gcn4 occupancies at a subset of 5' Gcn4 peaks in *snf2Δ\_I* cells.** (A) (i)-(iii) Heat maps depicting differences between *snf2Δ\_I* and WT\_I cells for (i) Gcn4 occupancies measured as in Fig 2A(iii), (ii) H3 occupancies surrounding the Gcn4 motifs of 5' sites from H3 ChIP-seq data, and (iii) Rpb3 occupancies averaged over the CDS of 5' genes, for the Gcn4 5' sites sorted by increasing order of fold-changes in Gcn4 occupancies in *snf2Δ P<sub>TET</sub>-STH1\_I* vs. WT\_I cells. (B) (i)-(iii) Same analyses shown in (A) except sorted by increasing order of fold-changes in Gcn4 occupancies in *snf2Δ\_I* vs. WT\_I cells. The locations of 5' Gcn4 peaks in quartiles 1, 2–3 and 4 for changes in Gcn4 binding in *snf2Δ\_I* vs. WT cells are indicated. (C) (i)-(iii) Same analyses shown in (A) except for *P<sub>TET</sub>-STH1\_I* vs. WT\_I data.

(DOCX)

**S12 Fig. Defective eviction of nucleosomes associated with reduced Gcn4 occupancies at a subset of 5' Gcn4 peaks in *ino80Δ\_I* cells.** (A) (i)-(iii) Heat maps depicting differences between *ino80Δ\_I* and WT\_I cells for (i) Gcn4 occupancies measured as in S6A(i) Fig, (ii) H3 occupancies surrounding the Gcn4 motifs of 5' sites from H3 ChIP-seq data, and (iii) Rpb3 occupancies averaged over the CDS of 5' genes, for Gcn4 5' sites sorted by increasing order of fold-changes in Gcn4 occupancies in *ino80Δ\_I* vs. WT\_I cells. (B-D) Notched box plots for the 3 sets of 5' sites defined in S6A(ii) Fig, and indicated again in panel A(ii), depicting (B) H3 occupancies per base pair in the ±100 bp windows surrounding the Gcn4 motifs, (C) log<sub>2</sub> Gcn4 occupancies taken from S6C Fig, and (D) log<sub>2</sub> Rpb3 occupancies averaged over the CDS of genes with 5' sites. H3 and Rpb3 occupancies were calculated from ChIP-seq data of sonicated chromatin from at least 3 biological replicates of WT\_U, WT\_I and *ino80Δ\_I* cells. *P* values from Mann-Whitney-Wilcoxon tests are indicated. The heat map of H3 occupancy changes conferred by *ino80Δ* around the 5' motifs ordered by the Gcn4 occupancy reductions in this mutant (panel A(i)) reveals that the 5' sites with the strongest reductions in Gcn4 binding in *ino80Δ* cells located at the top of the map (Set\_I) show the strongest increases in H3 occupancies centered around the Gcn4 motifs (panel A(ii)). Moreover, the decreases in median Gcn4 occupancy for individual 5' sites conferred by *ino80Δ* are paralleled by increased median H3 occupancies for the Set\_I group of 5' sites; whereas the sites in Set\_II and III show no significant changes in median H3 or Gcn4 occupancies in *ino80Δ\_I* versus WT\_I cells (panels 12B-C, Sets\_I-III, col. 3 vs. 2). The subset of genes with 5' sites that are most dependent on Ino80C for Gcn4 binding generally show the greatest reductions in Rpb3 occupancies (Set\_I sites in panel A (iii) vs. (i)). Moreover, the Set\_I genes, but not genes in Sets\_II-III, show reduced median occupancies of both Gcn4 and Rpb3 in *ino80Δ\_I* versus WT\_I cells (panels C-D(i)-(iii), col. 3 vs. 2). As only the Set\_I genes also exhibit increased median H3 occupancies in *ino80Δ\_I* cells (panel B(i)-(iii), col. 3 vs. 2), it seems likely that a defect in Gcn4 binding (and subsequent impaired recruitment of other coactivators) in combination with loss of Ino80C-mediated promoter nucleosome eviction produces the reduced transcription of Set\_I genes conferred by *ino80Δ*. (E) Gene browser profiles of Gcn4 and H3 occupancies from ChIP-seq analyses of sonicated chromatin for the indicated strains, as described in S4 Fig.

(DOCX)

**S13 Fig. Decreased TBP recruitment at 5' and ORF genes in *ino80Δ\_I* cells.** (A-B) Averaged TBP occupancies surrounding the Gcn4 motifs in ORF peaks from ChIP-seq data of sonicated

chromatin using anti-TBP antibodies from at least 2 biological replicates for the indicated mutant and WT strains. (C) Notched box plots of factor occupancies in the 83 5' gene promoters for the two bins defined in Fig 5C for (i)  $\log_2$  TBP within  $\pm 100$  bp of TBP peak summits and (ii) H3 within  $\pm 100$  bp of the TBP peak summits. *P* values from Mann-Whitney-Wilcoxon tests are indicated. (D-E) Gene browser profiles of TBP, Rpb3, and H3 occupancies from ChIP-seq analyses of sonicated chromatin for the indicated strains. The TBP occupancies per nucleotide over the TBP peaks and Rpb3 occupancies per nucleotide over the CDS are listed next to the relevant peaks or CDSs. The locations of the Gcn4 motifs and TBP summits are indicated with vertical hash marks, and the positions of -1 and +1 nucleosomes with dashes, at the bottom of each profile.

(DOCX)

**S14 Fig. Gene browser profiles of TBP, Rpb3, and H3 occupancies from ChIP-seq analyses of sonicated chromatin for the indicated strains.** The TBP occupancies per nucleotide over the TBP peaks and Rpb3 occupancies per nucleotide over the CDS are listed next to the relevant peaks or CDSs. The locations of the Gcn4 motifs and TBP summits are indicated with vertical hash marks, and the positions of -1 and +1 nucleosomes with dashes, at the bottom of each profile.

(DOCX)

**S15 Fig. Coactivator-redundant genes have a greater requirement than TFIID-dependent genes for RSC and Ino80C for TBP recruitment.** Changes in TBP occupancies surrounding the TSSs in the indicated mutants versus WT under non-starvation conditions are plotted for the coactivator-redundant and TFIID-dependent genes defined by Donczew et al. (2020), along with the corresponding changes for the RPGs.

(DOCX)

**S1 File. Annotations of the start and end coordinates of Gcn4 ChIP-seq occupancy peaks and of 200 bp intervals surrounding the peak summits of TBP ChIP-seq occupancy peaks.**

(XLSX)

**S2 File. Compilation of all data used to construct plots in both main and supplementary figures.**

(XLSX)

## Acknowledgments

We thank Razvan Chereji and David Clark for many helpful discussions, and Joseph Reese for his generous gift of TBP antibodies.

## Author Contributions

**Conceptualization:** Yashpal Rawal, Alan G. Hinnebusch.

**Data curation:** Yashpal Rawal.

**Formal analysis:** Yashpal Rawal, Hongfang Qiu, Alan G. Hinnebusch.

**Investigation:** Yashpal Rawal, Hongfang Qiu.

**Methodology:** Yashpal Rawal, Hongfang Qiu.

**Project administration:** Yashpal Rawal, Alan G. Hinnebusch.

**Resources:** Alan G. Hinnebusch.



**Supervision:** Alan G. Hinnebusch.

**Validation:** Yashpal Rawal.

**Visualization:** Yashpal Rawal, Hongfang Qiu.

**Writing – original draft:** Yashpal Rawal.

**Writing – review & editing:** Yashpal Rawal, Hongfang Qiu, Alan G. Hinnebusch.

## References

1. Jiang C, Pugh BF. Nucleosome positioning and gene regulation: advances through genomics. *Nat Rev Genet.* 2009; 10(3):161–72. Epub 2009/02/11. nrg2522 [pii] <https://doi.org/10.1038/nrg2522> PMID: 19204718.
2. Wang X, Bai L, Bryant GO, Ptashne M. Nucleosomes and the accessibility problem. *Trends Genet.* 2011; 27(12):487–92. Epub 2011/10/25. S0168-9525(11)00155-7 [pii] <https://doi.org/10.1016/j.tig.2011.09.001> PMID: 22019336.
3. Rando OJ, Winston F. Chromatin and transcription in yeast. *Genetics.* 2012; 190(2):351–87. Epub 2012/02/22. <https://doi.org/10.1534/genetics.111.132266> [pii] PMID: 22345607; PubMed Central PMCID: PMC3276623.
4. Cui F, Cole HA, Clark DJ, Zhurkin VB. Transcriptional activation of yeast genes disrupts intragenic nucleosome phasing. *Nucleic Acids Res.* 2012; 40(21):10753–64. Epub 2012/09/27. gks870 [pii] <https://doi.org/10.1093/nar/gks870> PMID: 23012262; PubMed Central PMCID: PMC3510488.
5. Devlin C, Tice-Baldwin K, Shore D, Arndt KT. RAP1 is required for BAS1/BAS2- and GCN4-dependent transcription of the yeast *UJHIS4* gene. *Mol Cell Biol.* 1991; 11:3642–51. <https://doi.org/10.1128/mcb.11.7.3642-3651.1991> PMID: 1904543
6. Yu L, Morse RH. Chromatin opening and transactivator potentiation by RAP1 in *Saccharomyces cerevisiae*. *Mol Cell Biol.* 1999; 19(8):5279–88. Epub 1999/07/20. <https://doi.org/10.1128/MCB.19.8.5279> PMID: 10409719; PubMed Central PMCID: PMC84371.
7. Levo M, Avnit-Sagi T, Lotan-Pompan M, Kalma Y, Weinberger A, Yakhini Z, et al. Systematic Investigation of Transcription Factor Activity in the Context of Chromatin Using Massively Parallel Binding and Expression Assays. *Mol Cell.* 2017; 65(4):604–17 e6. <https://doi.org/10.1016/j.molcel.2017.01.007> PMID: 28212748.
8. Boeger H, Griesenbeck J, Strattan JS, Kornberg RD. Nucleosomes unfold completely at a transcriptionally active promoter. *Mol Cell.* 2003; 11(6):1587–98. Epub 2003/06/25. [https://doi.org/10.1016/s1097-2765\(03\)00231-4](https://doi.org/10.1016/s1097-2765(03)00231-4) PMID: 12820971.
9. Reinke H, Horz W. Histones are first hyperacetylated and then lose contact with the activated PHO5 promoter. *Mol Cell.* 2003; 11(6):1599–607. [https://doi.org/10.1016/s1097-2765\(03\)00186-2](https://doi.org/10.1016/s1097-2765(03)00186-2) PMID: 12820972.
10. Reja R, Vinayachandran V, Ghosh S, Pugh BF. Molecular mechanisms of ribosomal protein gene coregulation. *Genes Dev.* 2015; 29(18):1942–54. <https://doi.org/10.1101/gad.268896.115> PMID: 26385964; PubMed Central PMCID: PMC4579351.
11. Nocetti N, Whitehouse I. Nucleosome repositioning underlies dynamic gene expression. *Genes Dev.* 2016; 30(6):660–72. <https://doi.org/10.1101/gad.274910.115> PMID: 26966245; PubMed Central PMCID: PMC4803052.
12. Rawal Y, Chereji RV, Qiu H, Ananthkrishnan S, Govind CK, Clark DJ, et al. SWI/SNF and RSC cooperate to reposition and evict promoter nucleosomes at highly expressed genes in yeast. *Genes Dev.* 2018; 32(9–10):695–710. <https://doi.org/10.1101/gad.312850.118> PMID: 29785963; PubMed Central PMCID: PMC6004078.
13. Krietenstein N, Wal M, Watanabe S, Park B, Peterson CL, Pugh BF, et al. Genomic Nucleosome Organization Reconstituted with Pure Proteins. *Cell.* 2016; 167(3):709–21 e12. <https://doi.org/10.1016/j.cell.2016.09.045> PMID: 27768892; PubMed Central PMCID: PMC5240917.
14. Kubik S, Bruzzone MJ, Challal D, Dreos R, Mattarocci S, Bucher P, et al. Opposing chromatin remodelers control transcription initiation frequency and start site selection. *Nat Struct Mol Biol.* 2019; 26(8):744–54. Epub 2019/08/07. <https://doi.org/10.1038/s41594-019-0273-3> PMID: 31384063.
15. Yen K, Vinayachandran V, Batta K, Koerber RT, Pugh BF. Genome-wide Nucleosome Specificity and Directionality of Chromatin Remodelers. *Cell.* 2012; 149(7):1461–73. Epub 2012/06/26. <https://doi.org/10.1016/j.cell.2012.04.036> [pii] PMID: 22726434; PubMed Central PMCID: PMC3397793.

16. Parnell TJ, Huff JT, Cairns BR. RSC regulates nucleosome positioning at Pol II genes and density at Pol III genes. *Embo J*. 2008; 27(1):100–10. <https://doi.org/10.1038/sj.emboj.7601946> PMID: 18059476.
17. Badis G, Chan ET, van Bakel H, Pena-Castillo L, Tillo D, Tsui K, et al. A library of yeast transcription factor motifs reveals a widespread function for Rsc3 in targeting nucleosome exclusion at promoters. *Mol Cell*. 2008; 32(6):878–87. <https://doi.org/10.1016/j.molcel.2008.11.020> PMID: 19111667; PubMed Central PMCID: PMC2743730.
18. Hartley PD, Madhani HD. Mechanisms that specify promoter nucleosome location and identity. *Cell*. 2009; 137(3):445–58. <https://doi.org/10.1016/j.cell.2009.02.043> PMID: 19410542.
19. Ganguli D, Chereji RV, Iben JR, Cole HA, Clark DJ. RSC-dependent constructive and destructive interference between opposing arrays of phased nucleosomes in yeast. *Genome Res*. 2014; 24(10):1637–49. <https://doi.org/10.1101/gr.177014.114> PMID: 25015381; PubMed Central PMCID: PMC4199373.
20. Parnell TJ, Schlichter A, Wilson BG, Cairns BR. The chromatin remodelers RSC and ISW1 display functional and chromatin-based promoter antagonism. *Elife*. 2015; 4:e06073. <https://doi.org/10.7554/eLife.06073> PMID: 25821983; PubMed Central PMCID: PMC4423118.
21. van Bakel H, Tsui K, Gebbia M, Mnaimneh S, Hughes TR, Nislow C. A compendium of nucleosome and transcript profiles reveals determinants of chromatin architecture and transcription. *PLoS Genet*. 2013; 9(5):e1003479. <https://doi.org/10.1371/journal.pgen.1003479> PMID: 23658529; PubMed Central PMCID: PMC3642058.
22. Brahma S, Udugama MI, Kim J, Hada A, Bhardwaj SK, Hailu SG, et al. INO80 exchanges H2A.Z for H2A by translocating on DNA proximal to histone dimers. *Nat Commun*. 2017; 8:15616. <https://doi.org/10.1038/ncomms15616> PMID: 28604691; PubMed Central PMCID: PMC5472786.
23. Jeronimo C, Watanabe S, Kaplan CD, Peterson CL, Robert F. The Histone Chaperones FACT and Spt6 Restrict H2A.Z from Intragenic Locations. *Mol Cell*. 2015; 58(6):1113–23. <https://doi.org/10.1016/j.molcel.2015.03.030> PMID: 25959393; PubMed Central PMCID: PMC4475440.
24. Mizuguchi G, Shen X, Landry J, Wu WH, Sen S, Wu C. ATP-driven exchange of histone H2AZ variant catalyzed by SWR1 chromatin remodeling complex. *Science*. 2004; 303(5656):343–8. <https://doi.org/10.1126/science.1090701> PMID: 14645854.
25. Rosonina E, Yurko N, Li W, Hoque M, Tian B, Manley JL. Threonine-4 of the budding yeast RNAP II CTD couples transcription with Htz1-mediated chromatin remodeling. *Proc Natl Acad Sci U S A*. 2014; 111(33):11924–31. Epub 2014/07/30. 1412802111 [pii] <https://doi.org/10.1073/pnas.1412802111> PMID: 25071213; PubMed Central PMCID: PMC4143052.
26. Qiu H, Biernat E, Govind CK, Rawal Y, Chereji RV, Clark DJ, et al. Chromatin remodeler Ino80C acts independently of H2A.Z to evict promoter nucleosomes and stimulate transcription of highly expressed genes in yeast. *Nucleic Acids Res*. 2020; 48(15):8408–30. Epub 2020/07/15. <https://doi.org/10.1093/nar/gkaa571> PMID: 32663283; PubMed Central PMCID: PMC7470979.
27. Rhee HS, Pugh BF. Genome-wide structure and organization of eukaryotic pre-initiation complexes. *Nature*. 2012; 483(7389):295–301. <https://doi.org/10.1038/nature10799> PMID: 22258509; PubMed Central PMCID: PMC3306527.
28. Klein-Brill A, Joseph-Strauss D, Appleboim A, Friedman N. Dynamics of Chromatin and Transcription during Transient Depletion of the RSC Chromatin Remodeling Complex. *Cell Rep*. 2019; 26(1):279–92 e5. Epub 2019/01/04. <https://doi.org/10.1016/j.celrep.2018.12.020> PMID: 30605682; PubMed Central PMCID: PMC6315372.
29. Kubik S, O'Duibhir E, de Jonge WJ, Mattarocci S, Albert B, Falcone JL, et al. Sequence-Directed Action of RSC Remodeler and General Regulatory Factors Modulates +1 Nucleosome Position to Facilitate Transcription. *Mol Cell*. 2018; 71(1):89–102 e5. <https://doi.org/10.1016/j.molcel.2018.05.030> PMID: 29979971.
30. Qiu H, Chereji RV, Hu C, Cole HA, Rawal Y, Clark DJ, et al. Genome-wide cooperation by HAT Gcn5, remodeler SWI/SNF, and chaperone Ydj1 in promoter nucleosome eviction and transcriptional activation. *Genome Res*. 2016; 26(2):211–25. <https://doi.org/10.1101/gr.196337.115> PMID: 26602697; PubMed Central PMCID: PMC4728374.
31. Barbaric S, Luckenbach T, Schmid A, Blaschke D, Horz W, Korber P. Redundancy of chromatin remodeling pathways for the induction of the yeast PHO5 promoter in vivo. *J Biol Chem*. 2007; 282(38):27610–21. <https://doi.org/10.1074/jbc.M700623200> PMID: 17631505.
32. Schwabish MA, Struhl K. The Swi/Snf complex is important for histone eviction during transcriptional activation and RNA polymerase II elongation in vivo. *Mol Cell Biol*. 2007; 27(20):6987–95. <https://doi.org/10.1128/MCB.00717-07> PMID: 17709398.
33. Sharma VM, Li B, Reese JC. SWI/SNF-dependent chromatin remodeling of RNR3 requires TAF(II)s and the general transcription machinery. *Genes Dev*. 2003; 17(4):502–15. <https://doi.org/10.1101/gad.1039503> PMID: 12600943.

34. Shivaswamy S, Iyer VR. Stress-dependent dynamics of global chromatin remodeling in yeast: dual role for SWI/SNF in the heat shock stress response. *Mol Cell Biol.* 2008; 28(7):2221–34. Epub 2008/01/24. <https://doi.org/10.1128/MCB.01659-07> [pii] PMID: 18212068; PubMed Central PMCID: PMC2268435.
35. Musladin S, Krietenstein N, Korber P, Barbaric S. The RSC chromatin remodeling complex has a crucial role in the complete remodeler set for yeast PHO5 promoter opening. *Nucleic Acids Res.* 2014; 42(7):4270–82. Epub 2014/01/28. gkt1395 [pii] <https://doi.org/10.1093/nar/gkt1395> PMID: 24465003; PubMed Central PMCID: PMC3985623.
36. Gowans GJ, Schep AN, Wong KM, King DA, Greenleaf WJ, Morrison AJ. INO80 Chromatin Remodeling Coordinates Metabolic Homeostasis with Cell Division. *Cell Rep.* 2018; 22(3):611–23. Epub 2018/01/19. <https://doi.org/10.1016/j.celrep.2017.12.079> PMID: 29346761; PubMed Central PMCID: PMC5949282.
37. Klopff E, Schmidt HA, Clauder-Munster S, Steinmetz LM, Schuller C. INO80 represses osmotic stress induced gene expression by resetting promoter proximal nucleosomes. *Nucleic Acids Res.* 2017; 45(7):3752–66. <https://doi.org/10.1093/nar/gkw1292> PMID: 28025392; PubMed Central PMCID: PMC5397147.
38. Xue Y, Pradhan SK, Sun F, Chronis C, Tran N, Su T, et al. Mot1, Ino80C, and NC2 Function Coordinately to Regulate Pervasive Transcription in Yeast and Mammals. *Mol Cell.* 2017; 67(4):594–607 e4. <https://doi.org/10.1016/j.molcel.2017.06.029> PMID: 28735899; PubMed Central PMCID: PMC5573681.
39. Mehta GD, Ball DA, Eriksson PR, Chereji RV, Clark DJ, McNally JG, et al. Single-Molecule Analysis Reveals Linked Cycles of RSC Chromatin Remodeling and Ace1p Transcription Factor Binding in Yeast. *Mol Cell.* 2018; 72(5):875–87 e9. Epub 2018/10/16. <https://doi.org/10.1016/j.molcel.2018.09.009> PMID: 30318444; PubMed Central PMCID: PMC6289719.
40. Adkins MW, Williams SK, Linger J, Tyler JK. Chromatin disassembly from the PHO5 promoter is essential for the recruitment of the general transcription machinery and coactivators. *Mol Cell Biol.* 2007; 27(18):6372–82. Epub 2007/07/11. <https://doi.org/10.1128/MCB.00981-07> PMID: 17620413; PubMed Central PMCID: PMC2099613.
41. Li M, Hada A, Sen P, Olufemi L, Hall MA, Smith BY, et al. Dynamic regulation of transcription factors by nucleosome remodeling. *Elife.* 2015; 4. Epub 2015/06/06. <https://doi.org/10.7554/eLife.06249> PMID: 26047462; PubMed Central PMCID: PMC4456607.
42. Nagaich AK, Walker DA, Wolford R, Hager GL. Rapid periodic binding and displacement of the glucocorticoid receptor during chromatin remodeling. *Mol Cell.* 2004; 14(2):163–74. Epub 2004/04/22. [https://doi.org/10.1016/s1097-2765\(04\)00178-9](https://doi.org/10.1016/s1097-2765(04)00178-9) PMID: 15099516.
43. Jia MH, Larossa RA, Lee JM, Rafalski A, Derose E, Gonye G, et al. Global expression profiling of yeast treated with an inhibitor of amino acid biosynthesis, sulfometuron methyl. *Physiol Genomics.* 2000; 3:83–92. <https://doi.org/10.1152/physiolgenomics.2000.3.2.83> PMID: 11015603
44. Natarajan K, Meyer MR, Jackson BM, Slade D, Roberts C, Hinnebusch AG, et al. Transcriptional profiling shows that Gcn4p is a master regulator of gene expression during amino acid starvation in yeast. *Molecular and Cellular Biology.* 2001; 21(13):4347–68. <https://doi.org/10.1128/MCB.21.13.4347-4368.2001> WOS:000169233400026. PMID: 11390663
45. Saint M, Sawhney S, Sinha I, Singh RP, Dahiya R, Thakur A, et al. The TAF9 C-terminal conserved region domain is required for SAGA and TFIID promoter occupancy to promote transcriptional activation. *Mol Cell Biol.* 2014; 34(9):1547–63. Epub 2014/02/20. <https://doi.org/10.1128/MCB.01060-13> PMID: 24550006; PubMed Central PMCID: PMC3993605.
46. Rawal Y, Chereji RV, Valabhaju V, Qiu H, Ocampo J, Clark DJ, et al. Gcn4 Binding in Coding Regions Can Activate Internal and Canonical 5' Promoters in Yeast. *Mol Cell.* 2018; 70(2):297–311 e4. <https://doi.org/10.1016/j.molcel.2018.03.007> PMID: 29628310.
47. Liu X, Lee CK, Granek JA, Clarke ND, Lieb JD. Whole-genome comparison of Leu3 binding in vitro and in vivo reveals the importance of nucleosome occupancy in target site selection. *Genome Res.* 2006; 16(12):1517–28. <https://doi.org/10.1101/gr.5655606> PMID: 17053089; PubMed Central PMCID: PMC1665635.
48. Natarajan K, Jackson BM, Zhou H, Winston F, Hinnebusch AG. Transcriptional activation by Gcn4p involves independent interactions with the SWI/SNF complex and SRB/mediator. *MolCell.* 1999; 4:657–64. [https://doi.org/10.1016/s1097-2765\(00\)80217-8](https://doi.org/10.1016/s1097-2765(00)80217-8) PMID: 10549298
49. Swanson MJ, Qiu H, Sumibcay L, Krueger A, Kim S-J, Natarajan K, et al. A Multiplicity of coactivators is required by Gcn4p at individual promoters in vivo. *MolCellBiol.* 2003; 23(8):2800–20. <https://doi.org/10.1128/MCB.23.8.2800-2820.2003> PMID: 12665580
50. Kuang Z, Cai L, Zhang X, Ji H, Tu BP, Boeke JD. High-temporal-resolution view of transcription and chromatin states across distinct metabolic states in budding yeast. *Nat Struct Mol Biol.* 2014; 21

- (10):854–63. Epub 2014/09/01. nsmc.2881 [pii] <https://doi.org/10.1038/nsmb.2881> PMID: 25173176; PubMed Central PMCID: PMC4190017.
51. Donczew R, Warfield L, Pacheco D, Erijman A, Hahn S. Two roles for the yeast transcription coactivator SAGA and a set of genes redundantly regulated by TFIID and SAGA. *Elife*. 2020; 9. Epub 2020/01/09. <https://doi.org/10.7554/eLife.50109> PMID: 31913117; PubMed Central PMCID: PMC6977968.
  52. Neely KE, Hassan AH, Wallberg AE, Steger DJ, Cairns BR, Wright AP, et al. Activation Domain-Mediated Targeting of the SWI/SNF Complex to Promoters Stimulates Transcription from Nucleosome Arrays. *Arrays Mol Cell*. 1999; 4:649–55. [https://doi.org/10.1016/s1097-2765\(00\)80216-6](https://doi.org/10.1016/s1097-2765(00)80216-6) PMID: 10549297
  53. Qiu H, Hu C, Zhang F, Hwang GJ, Swanson MJ, Boonchird C, et al. Interdependent recruitment of SAGA and Srb mediator by transcriptional activator Gcn4p. *Mol Cell Biol*. 2005; 25(9):3461–74. <https://doi.org/10.1128/MCB.25.9.3461-3474.2005> PMID: 15831453.
  54. Bunker CA, Kingston RE. Transcriptional repression by Drosophila and mammalian Polycomb group proteins in transfected mammalian cells. *Mol Cell Biol*. 1994; 14(3):1721–32. Epub 1994/03/01. <https://doi.org/10.1128/mcb.14.3.1721-1732.1994> PubMed Central PMCID: PMC358530. PMID: 7906858
  55. Vashee S, Kodadek T. The activation domain of GAL4 protein mediates cooperative promoter binding with general transcription factors. *Proc Natl Acad Sci USA*. 1995; 92:10683–7. <https://doi.org/10.1073/pnas.92.23.10683> PMID: 7479865
  56. Qiu H, Hu C, Yoon S, Natarajan K, Swanson MJ, Hinnebusch AG. An array of coactivators is required for optimal recruitment of TATA binding protein and RNA polymerase II by promoter-bound Gcn4p. *Mol Cell Biol*. 2004; 24(10):4104–17. <https://doi.org/10.1128/MCB.24.10.4104-4117.2004> PMID: 15121833.
  57. Kim Y, McLaughlin N, Lindstrom K, Tsukiyama T, Clark DJ. Activation of *Saccharomyces cerevisiae* HIS3 results in Gcn4p-dependent, SWI/SNF-dependent mobilization of nucleosomes over the entire gene. *Mol Cell Biol*. 2006; 26(22):8607–22. Epub 2006/09/20. <https://doi.org/10.1128/MCB.00678-06> PMID: 16982689; PubMed Central PMCID: PMC1636772.
  58. Longtine MS, McKenzie A III, Demarini DJ, Shah NG, Wach A, Brachat A, et al. Additional modules for versatile and economical PCR-based gene deletion and modification in *Saccharomyces cerevisiae*. *Yeast*. 1998; 14:953–61. [https://doi.org/10.1002/\(SICI\)1097-0061\(199807\)14:10<953::AID-YEA293>3.0.CO;2-U](https://doi.org/10.1002/(SICI)1097-0061(199807)14:10<953::AID-YEA293>3.0.CO;2-U) PMID: 9717241
  59. Zhang F, Gaur NA, Hasek J, Kim SJ, Qiu H, Swanson MJ, et al. Disrupting vesicular trafficking at the endosome attenuates transcriptional activation by Gcn4. *Mol Cell Biol*. 2008; 28(22):6796–818. <https://doi.org/10.1128/MCB.00800-08> PMID: 18794364.
  60. Langmead B, Salzberg SL. Fast gapped-read alignment with Bowtie 2. *Nat Methods*. 2012; 9(4):357–9. Epub 2012/03/06. <https://doi.org/10.1038/nmeth.1923> PMID: 22388286; PubMed Central PMCID: PMC3322381.
  61. Robinson JT, Thorvaldsdottir H, Winckler W, Guttman M, Lander ES, Getz G, et al. Integrative genomics viewer. *Nat Biotechnol*. 2011; 29(1):24–6. <https://doi.org/10.1038/nbt.1754> PMID: 21221095; PubMed Central PMCID: PMC3346182.
  62. Pelechano V, Wei W, Steinmetz LM. Extensive transcriptional heterogeneity revealed by isoform profiling. *Nature*. 2013; 497(7447):127–31. <https://doi.org/10.1038/nature12121> PMID: 23615609; PubMed Central PMCID: PMC3705217.